Hindawi Publishing Corporation
Advances in High Energy Physics
Volume 2014, Article ID 681312, 19 pages
http://dx.doi.org/10.1155/2014/681312

Review Article

New Directions in Direct Dark Matter Searches

Paolo Panci

Institut d'Astrophysique, CNRS, UMR 7095 & Université Pierre et Marie Curie, 98 bis Boulevard Arago, 75014 Paris, France

Correspondence should be addressed to Paolo Panci; pancipaolo@gmail.com

Received 9 January 2014; Accepted 3 February 2014; Published 16 April 2014

Academic Editor: Anselmo Meregaglia

I present the status of direct dark matter detection with specific attention to the experimental results and their phenomenological interpretation in terms of dark matter interactions. In particular I review a new and more general approach to study signals in this field based on nonrelativistic operators which parametrize more efficiently the dark matter-nucleus interactions in terms of a very limited number of relevant degrees of freedom. Then I list the major experimental results, pointing out the main uncertainties that affect the theoretical interpretation of the data. Finally, since the underlying theory that describes both the dark matter and the standard model fields is unknown, I address the uncertainties coming from the nature of the interaction. In particular, the phenomenology of a class of models in which the interaction between dark matter particles and target nuclei is of a long range type is discussed.

1. Introduction

One of the most exciting open questions at the interface between particle physics and cosmology is the nature of Dark Matter (DM). The first person who provided evidence and inferred the presence of DM was a Swiss-American astrophysicist, Fritz Zwicky. He applied the virial theorem to the Coma cluster of galaxies and obtained evidence of unseen mass. Roughly 40 years following the discoveries of Zwicky and others, Vera Rubin and collaborators conducted an extensive study of the rotation curves of isolated spiral galaxies. They announced the discovery that the rotational curves of stars in spiral galaxies exhibit a characteristic flat behaviour at large distance in contrast with Kepler's law. Many other evidence of unseen mass on distance scales of the size of galaxies and clusters of galaxies appeared throughout the years, but the most precise measurement of the total amount of DM comes from cosmological scales. In particular, the measurements of modern precision cosmology (the Cosmic Microwave Background (CMB) and the surveys of the Large Scale Structure (LSS) of the Universe) provide the current most relevant evidence. Apart from the qualitative agreement, it is the quantitative fitting of the wealth of available data that allows the amount of DM to be one of the cosmological parameters now most precisely measured ($\Omega_\chi h^2 = 0.1199 \pm 0.0027$; see [1, Table 2]). Therefore, we have compelling evidence of unseen mass, but the microscopic features of this new kind of matter remain unknown yet. Direct and indirect searches may shed light on the nature of DM, and therefore a careful study of their phenomenology is fundamental. For a pedagogical review on this subject, see, for example, [2].

Direct searches for DM aim at detecting the nuclear recoils arising from scattering between DM particles and target nuclei in underground detectors. DM direct detection experiments are providing exciting results in terms of measured features which have the right properties to be potentially ascribed to a DM signal. For example in addition to the long-standing DAMA results, nowadays there are other experiments, such as CoGeNT, CRESST-II, and CDMS-Si that start to see some anomalies in their counting rates. On the other hand, the situation in this field is extremely unclear and confusing, because, on top of these positive result experiments, the constraints coming from null results, like XENON100, COUPP, PICASSO and very recently LUX, are very stringent and put the interpretation of the anomalies in terms of a DM interaction in serious trouble. Nevertheless, there are at least two main caveats when the results from the experiments commented upon above are interpreted. The first is that one has to

treat with great care the fine experimental details associated with the results quoted by each experiment. The second caveat is instead associated with the interpretation of the data within a very simple-minded DM model. For instance, the DM-nucleus spin independent contact interaction is just a benchmark example. Upon relaxing some of these assumptions, the current complicated experimental puzzle can probably be solved.

The *scope of this work* is to present the *status* of direct DM detection with specific attention to the experimental results and their phenomenological interpretation in terms of DM interaction. In particular in Section 2, I review a new and more general approach to study signals in this field based on nonrelativistic operators which parameterize most efficiently the DM-nucleus interactions in terms of a very limited number of relevant degrees of freedom. In Section 3, I review the experimental results and their interpretation in terms of the "standard" spin independent (SI) interaction. I list then the main uncertainties that affect the theoretical interpretation of the data: this is a very promising area of research since only major advancements here can probably reconcile the complicated puzzle showed by the experiments up. Finally in Section 4, I pose my attention on the uncertainties coming from the nature of the interaction. In particular the phenomenology of a class of models in which the interaction between DM particles and target nuclei is of a long range type is discussed.

2. Basics of Direct Detection Computations

2.1. Kinematics. As already stated, when a DM particle scatters off a nucleus, depending on the DM properties, one can envision at least two distinct kinematics, the elastic and the inelastic one. The elastic scattering is represented by

$$\chi + \mathcal{N}(A_{\mathcal{N}}, Z_{\mathcal{N}})_{\text{at rest}} \longrightarrow \chi + \mathcal{N}(A_{\mathcal{N}}, Z_{\mathcal{N}})_{\text{recoil}}, \quad (1)$$

while the inelastic is

$$\chi + \mathcal{N}(A_{\mathcal{N}}, Z_{\mathcal{N}})_{\text{at rest}} \longrightarrow \chi' + \mathcal{N}(A_{\mathcal{N}}, Z_{\mathcal{N}})_{\text{recoil}}. \quad (2)$$

In (1) and (2), χ and χ' are two DM particle states, and $A_{\mathcal{N}}$, $Z_{\mathcal{N}}$ are, respectively, the mass and atomic numbers of the nucleus $\mathcal{N}$.

We know, thanks to rotational curves data, that the velocity of χ in the vicinity of the Earth is of the order of $10^{-3}c$. Hence the scattering between a DM particle with velocity v and mass m_χ and a nucleus at rest with mass $m_{\mathcal{N}}$ occurs in deeply nonrelativistic regime. This is analogous with the collision between two billiard balls and therefore the recoil energy can be simply obtained by considering energy and momenta conservation separately. In the detector rest frame, such scattering would end up into a nuclear recoil of energy:

$$E_R = \frac{2\mu_{\chi\mathcal{N}}^2}{m_{\mathcal{N}}} v^2 \left(\frac{1 - \left(v_t^2/2v^2\right) - \sqrt{1 - \left(v_t^2/v^2\right)}\ \cos\theta}{2} \right),$$
$$v_t = 0, \text{ elastic scattering},$$
$$v_t \neq 0, \text{ inelastic scattering}, \quad (3)$$

where $\mu_{\chi\mathcal{N}} = m_\chi m_{\mathcal{N}}/(m_\chi + m_{\mathcal{N}})$ is the DM-nucleus reduced mass, θ as usual is the scattering angle in the center-of-mass frame, and $v_t = \sqrt{2\delta/\mu_{\chi\mathcal{N}}}$ is a threshold velocity. Here $\delta = m'_\chi - m_\chi$ is the mass splitting between χ and χ', and the equation above holds for $\delta \ll m'_\chi, m_\chi$. Elastic scattering occurs for $\delta = 0$, while $\delta \neq 0$ implies inelastic scattering. The minimal DM velocity providing the E_R recoil energy can be then obtained by putting $\theta = -\pi$ in (3). One gets

$$v_{\min}(E_R) = \sqrt{\frac{m_{\mathcal{N}} E_R}{2\mu_{\chi\mathcal{N}}^2}} \left(1 + \frac{\mu_{\chi\mathcal{N}}\delta}{m_{\mathcal{N}} E_R}\right). \quad (4)$$

2.2. Formalism of Nonrelativistic Operators. Having a disposal the basic quantity $v_{\min}$ that fully describes the kinematics of the DM-nucleus scatterings in (1) and (2) and the differential rate of nuclear recoil expected in a given detector can be achieved by weighting the differential cross section $d\sigma_{\mathcal{N}}/dE_R$ with the DM velocity distribution $f_E(\vec{v})$ in the velocity range allowed by the kinematics. It reads as follows:

$$\frac{dR_{\mathcal{N}}}{dE_R} = \frac{\xi_{\mathcal{N}}}{m_{\mathcal{N}}} \frac{\rho_\odot}{m_\chi} \int_{v_{\min}(E_R)}^{v_{\text{esc}}} d^3v v f_E(\vec{v}) \frac{d\sigma_{\mathcal{N}}}{dE_R}(v, E_R), \quad (5)$$

where $\xi_{\mathcal{N}}$ are the mass fractions of different nuclides ($\xi_{\mathcal{N}} = 10^3 N_A m_{\mathcal{N}} \zeta_{\mathcal{N}}/\text{kg}\ \overline{A}$, where $N_A = 6.022 \times 10^{23}$ is Avogadro's number, $\zeta_{\mathcal{N}}$ are the numeric abundances and $\overline{A} \equiv \sum_{\mathcal{N}} \zeta_{\mathcal{N}} A_{\mathcal{N}}$.), and $\rho_\odot \simeq 0.3\,\text{GeV/cm}^3$ is the DM energy density at the Earth's location. This is the canonical value routinely adopted in the literature (see, e.g., [2–4]). Recent computations have found a higher central value of it, still subject for some debate [5–7]. The integral in the right-hand side of the equation above is a key ingredient because it contains all the information related to the geometry of the DM halo, the nature of the DM-nucleus interaction, and in turn the nuclear response of the target. In the following we present the formalism of nonrelativistic (NR) operators and then we describe how to write down the main observables in terms of it.

(i) As already stated, the weight of the velocity integral is the DM velocity distribution $f_E(\vec{v})$. In the rest frame of our Galaxy it can be roughly approximated with a Maxwell-Boltzmann distribution due to the fact, as pointed out in [8], that the violent relaxation of the gravitational potential at the formation of the Milky Way leads to fast mixing of the DM

phase space elements. Therefore, DM particles were basically frozen in high-entropy configuration which are indeed Maxwell-Boltzmann-like. This has been roughly confirmed by some recent numeral simulation, but as one can see in [9, Figure 2], there are some deviations due to the DM assembly history of the Milky Way. Indeed one can see different features both at low and high velocities that of course are not present in the case of a Maxwell-Boltzmann distribution. Furthermore the geometry of the halo predicted by this kind of numerical simulation is not exactly spherical but tends to a triaxial configuration (see, e.g., [10]).

Keeping in mind that this is not the truth because we have not directly measured the properties of the DM halo yet, what we know for sure is that, since we are setting in the Earth laboratory frame, one has to boost the DM-nucleus relative velocity with the drift velocity of the Sun around the galactic center and the Earth's orbital velocity projected in the galactic plane. Therefore the DM velocity distribution $f_E(\vec{v})$ in the Earth frame is related to the DM velocity distribution in the galactic one $f_G(\vec{w})$ by the Galilean velocity transformation $f_E(\vec{v}) = f_G(\vec{v} + \vec{v}_E(t))$, where

$$\vec{v}_E(t) = \vec{v}_\odot + \vec{v}_\oplus(t). \tag{6}$$

Here $\vec{v}_\odot = \vec{v}_G + \vec{v}_S$ is the sum of the galactic rotational velocity of the local system $\vec{v}_G = (0, v_0, 0)$ (here $v_0 \simeq 220 \pm 50$ km/s is the local DM velocity) and the Sun's proper motion $\vec{v}_S \simeq (10, 13, 7)$ km/s with absolute value $v_\odot = 233 \pm 50$ km/s, while $\vec{v}_\oplus(t)$ is the time dependent Earth's orbital velocity with period of one year, phase around June 2nd (when it is aligned to $\vec{v}_\odot$), and size $v_\oplus \simeq 30$ km/s, and it is inclined of an angle $\gamma \simeq 60^\circ$ with respect to the galactic plane. More details can be found in [11–13]. Since in (6) the Earth's orbital velocity projected in the galactic plane $v_\oplus \cos\gamma$ is relatively small compared to $v_\odot$, we can approximate $\vec{v}_E(t)$ with its component directed toward the galactic center. We can then write

$$v_E(t) \simeq v_\odot + \Delta v \cos\left[\frac{2\pi(t-\phi)}{\tau}\right], \tag{7}$$

where $\Delta v = v_\oplus \cos\gamma \simeq 15$ km/s. Here $\phi \simeq 152.5$ days (June 2nd) is the phase and $\tau \simeq 365$ days is the period of the Earth motion around the Sun.

Therefore, in general, it is expected an annual modulation in the counting rate of direct detection experiment, as the incoming flux of DM particles toward us contains small oscillatory terms due to the Earth's proper motion around the Sun during the years. More details on this model independent signature can be found, for instance, in [14, 15]. It is worth stressing that looking for an annual modulation of the counting rate in direct detection is very challenging from the experimental point of view, simply because the modulus of the time dependent component of the velocity is relatively small compared to the constant one; in better words, the size of the modulated signal that experiments like DAMA and CoGeNT are looking for is suppressed with respect to the unmodulated one, due basically to the collective motion of the Solar system around the galactic center.

(ii) In the nonrelativistic limit the differential cross section can be written in the usual form:

$$\frac{d\sigma_{\mathcal{N}}}{dE_R}(v, E_R) = \frac{1}{32\pi}\frac{1}{m_\chi^2 m_{\mathcal{N}}}\frac{1}{v^2}\overline{|\mathcal{M}_{\mathcal{N}}|^2}, \tag{8}$$

where $\overline{|\mathcal{M}_{\mathcal{N}}|^2}$ is the DM-nucleus matrix element that encodes all the information related to the nuclear physics and the nature of the interactions. Since, as already stated, the velocity of the DM particles in the vicinity of the Earth is much smaller than the speed of light, the framework of relativistic quantum field theory is not too much appropriate to study signals in this field, especially if we do not have any clue about the underlying theory that describes the DM-quark interactions. A more useful and general framework is actually the one based on nonrelativistic operators. Indeed, since, for the elastic scattering, the relevant degrees of freedom are the DM-nucleon relative velocity $\vec{v}$, the exchanged momentum $\vec{q}$, the nucleon spin $\vec{s}_N$ ($N = p, n$ can be proton or neutron), and the DM one $\vec{s}_\chi$ (if different from zero), the scattering amplitude will then be a rotationally invariant function of this variables. In this regard, with $\vec{v}$, $\vec{q}$, $\vec{s}_N$, and $\vec{s}_\chi$ [16], we can construct a basis for 16 operators, which includes all possible spin configurations (the complete list and the numbering of the nonrelativistic operators can be found in [17–19]). The DM-nucleon matrix element can then be written as a linear combination of these operators, with coefficients that may depend on the momenta only through the q^2 or v^2 scalars (DM models feature a long range interaction with the Standard Model fermions provide perhaps the most notable example. Indeed, in this case, the differential cross section is enhanced at smaller exchanged momenta, due to the negative power dependence of q. A specific realization is offered by models in which DM particles can carry small but nonzero electric charge, electric dipole moment, or magnetic one. Their phenomenology in the context of DM direct searches has been studied in [20–31] and references therein.). In particular it reads

$$\mathcal{M}_N = \sum_{i=1}^{16} \mathfrak{c}_i^N(\lambda, m_\chi)\,\mathcal{O}_i^{\mathrm{NR}}, \tag{9}$$

where the coefficients $\mathfrak{c}_i^N$ are functions of the free parameters of the underlying relativistic theory, such as mediator masses, mixing angles, and couplings constants (collectively denoted by λ), and the DM mass m_χ. For instance, if the interaction between

a fermionic DM χ and the nucleon N is described by the "standard" SI Lagrangian $g_N/\Lambda^2\ \overline{\chi}\chi\ \overline{N}N$, the only nonrelativistic operator involved will be the identity ($\mathcal{O}_1^{\mathrm{NR}} = \mathbb{1}$). Before moving on, it is worth stressing that the operators above, which entirely describe the nonrelativistic physics of the DM-nucleus scattering, are many and they can either depend on the exchanged momenta $\vec{q}$ or the relative velocity $\vec{v}$. As a consequence, focussing on just one operator (e.g., $\mathcal{O}_1^{\mathrm{NR}}$) is not the most model independent way to study signals in direct DM searches, since theories can predict several operators entering together with the possibility that some of them may even interfere.

Since now the nucleus is of course made of protons and neutrons, one has to correct the DM-nucleon matrix element (9) with the nuclear responses, which are a sort of form factors that take account of the finite size of the target nuclei. According to [17, Equation (55)] we can then write the spin-averaged amplitude squared for scattering off a target nucleus $\mathcal{N}$ with mass $m_{\mathcal{N}}$ as

$$\overline{\left|\mathcal{M}_{\mathcal{N}}\right|^2} = \frac{m_{\mathcal{N}}^2}{m_N^2}\sum_{i,j=1}^{16}\sum_{N,N'=p,n} c_i^N c_j^{N'} F_{i,j}^{(N,N')}. \tag{10}$$

The $F_{i,j}^{(N,N')}(v, E_R, \mathcal{N})$ are the nuclear responses and they depend critically on the type of scattering nucleus $\mathcal{N}$: they are also functions of m_χ, v, and the nuclear recoil energy $E_R = q^2/2m_{\mathcal{N}}$. In Figure 1, the nuclear responses for both light element (on the left panel) and heavy one (on the right panel), considering two completely different kinds of interactions, are depicted. On a more specific level, in thick red the total nuclear response for the standard SI interaction is shown. As we can see, in the energy range of interest in direct DM experiments (few keV), it is enhanced by the canonical $A_{\mathcal{N}}^2$ factor: this is due to the fact that, in this case, the incoming DM particles see the nucleus as a point-like object with $A_{\mathcal{N}}$ scatter centers. On the other hand, we show in blue the nuclear responses of a completely different type of interaction which is both momenta and spin dependent ($\mathcal{O}_6^{\mathrm{NR}} = (\vec{s}_\chi \cdot \vec{q})(\vec{s}_N \cdot \vec{q})$). This type of interaction can give rise if the DM-nucleus interaction is mediated by a pseudoscalar particle. We can see that the nuclear responses are dominated by the scattering with protons, simply because neither the fluorine nor the iodine has unpaired neutrons and moreover the interaction goes to zero in the small momenta transferred limit.

A complete set of these nuclear responses for each pair of nucleons (N, N'), each pair of nonrelativistic operators (i, j), and for several target nuclei $\mathcal{N}$ has been provided in the appendices of [17]. This is extremely useful because, for the first time, different types of interactions can be studied in a more general ground. However, since this kind of computations is quite new, the uncertainties, especially for the spin, momenta, and velocity dependent interactions, are still quite large.

Having a disposal the general relation of the DM-nucleus matrix element (10), the differential cross section (8), and in turn the rate of nuclear recoil (5) can be rewritten, following [32], in a very general way. It reads

$$\frac{\mathrm{d}R_{\mathcal{N}}}{\mathrm{d}E_R} = X\xi_{\mathcal{N}}\sum_{i,j=1}^{16}\sum_{N,N'=p,n} c_i^N\left(\lambda, m_\chi\right) \times c_j^{N'}\left(\lambda, m_\chi\right)\mathcal{F}_{i,j}^{(N,N')}\left(E_R, \mathcal{N}\right), \tag{11}$$

where we defined

$$X \equiv \frac{\rho_\odot}{m_\chi}\frac{1}{32\pi}\frac{1}{m_\chi^2 m_N^2}, \tag{12}$$

$$\mathcal{F}_{i,j}^{(N,N')}\left(E_R, \mathcal{N}\right) \equiv \int_{v_{\min(E_R)}}^{v_{\mathrm{esc}}} \mathrm{d}^3 v \frac{1}{v} f_G\left(\vec{v} + \vec{v}_E(t)\right) F_{i,j}^{(N,N')}\left(v, E_R, \mathcal{N}\right). \tag{13}$$

2.2.1. "Standard" SI Contact Interaction. To give a concrete example, in the following the coefficient and the nuclear responses for the "standard" SI contact interaction are showed explicitly. In particular, when experiments present results in terms of this interaction, they implicitly assume (probably inspired by supersymmetric neutralino scattering) the following DM-nucleon effective Lagrangian:

$$\mathscr{L}_{\mathrm{SI}}^N = \lambda_{\mathrm{SI}}^N \overline{\chi}\chi\overline{N}N. \tag{14}$$

From this the DM-nucleon matrix element can be obtained by contracting (14) with initial and final states of the scattering. Performing then the nonrelativistic limit one gets

$$\mathcal{M}_{\mathrm{SI}}^N \equiv \left\langle \chi N \left| \mathscr{L}_{\mathrm{SI}}^N \right| \chi N \right\rangle \simeq 4\lambda_{\mathrm{SI}}^N m_\chi m_N \mathcal{O}_1^{\mathrm{NR}}, \tag{15}$$

where $\mathcal{O}_1^{\mathrm{NR}} = \mathbb{1}$ is the operator that describes the nonrelativistic limit of (14) and the coefficient is obviously given by $c_1^N(\lambda_{\mathrm{SI}}^N, m_\chi) = 4\lambda_{\mathrm{SI}}^N m_\chi m_N$.

For the SI scattering, DM-proton and DM-neutron couplings are customarily assumed to be equal and thus $\lambda_{\mathrm{SI}}^p = \lambda_{\mathrm{SI}}^n \equiv \lambda_{\mathrm{SI}}$ (isospin violating process is not taken into account). Plugging back then the coefficient in the general equation (11) and defining $\sigma_{\mathrm{SI}} = \lambda_{\mathrm{SI}}^2/\pi \cdot \mu_N^2$ (μ_N is the DM-nucleon reduced mass) to make contact with the usual physical cross sections, the differential rate of nuclear recoil reduces to the very well-know compact form:

$$\frac{\mathrm{d}R_{\mathcal{N}}}{\mathrm{d}E_R} = \frac{\xi_{\mathcal{N}}}{m_{\mathcal{N}}}\frac{\rho_\odot}{m_\chi}\left[\frac{m_{\mathcal{N}}}{2\mu_N^2}\sigma_{\mathrm{SI}}F_{\mathcal{N}}^{\mathrm{tot}}\left(E_R\right)\mathcal{J}\left(E_R\right)\right], \tag{16}$$

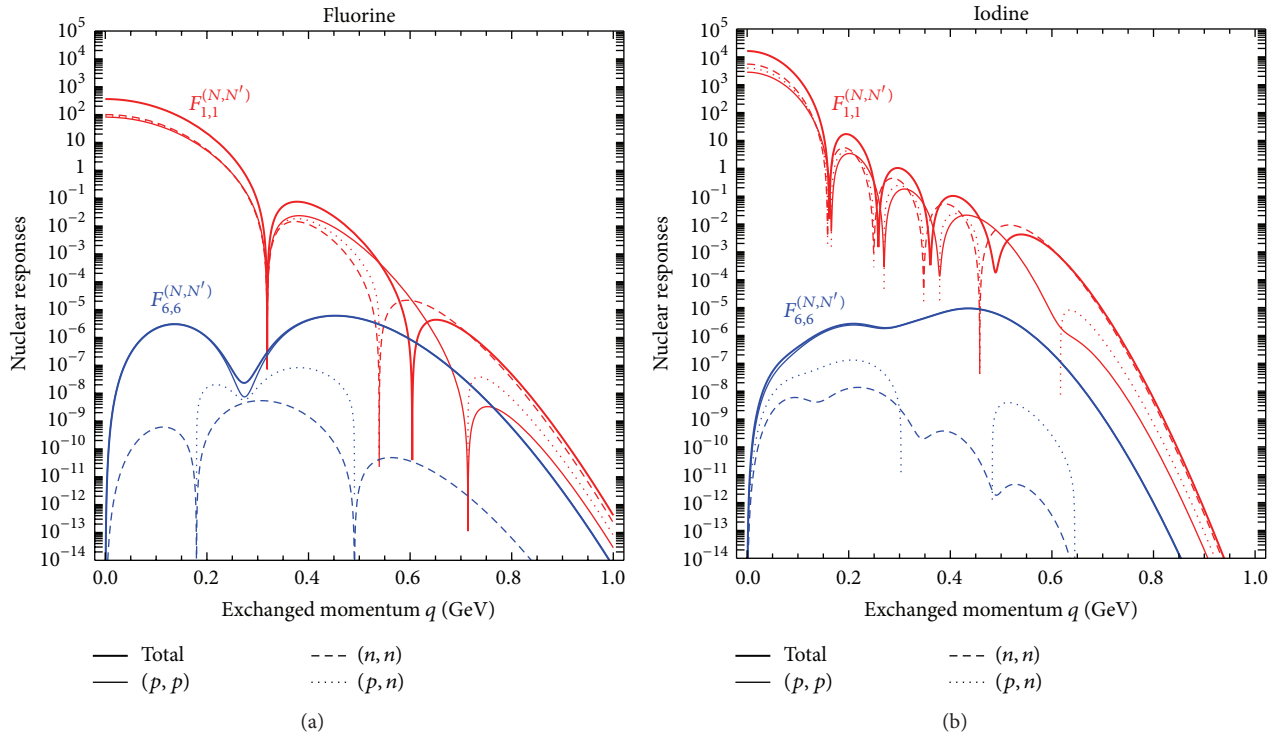

FIGURE 1: *Nuclear responses* of the fluorine (a) and the iodine (b) targets considering two completely different types of interactions. On a more specific level, we show, in red, the nuclear responses for the "standard" SI contact interaction, while in blue those for another kind of interaction described in the nonrelativistic limit by the operator $\mathcal{O}_6^{\mathrm{NR}} = (\vec{s}_\chi \cdot \vec{q})(\vec{s}_N \cdot \vec{q})$. The different hatching refers instead to the possible choices of nucleon pairs in the nucleus. In particular, the solid, dashed, and dotted lines are for (p,p), (n,n), and (p,n) pairs, while the thick ones are obtained by summing over all of them (total nuclear responses). Notice that the total nuclear responses for the "standard" SI contact interaction (thick red lines) reduce to $A_{\mathcal{N}}^2 F_{\mathrm{Helm}}^2(q)$, where $F_{\mathrm{Helm}}^2(q)$ is the customary Helm form factor [33].

where we define the total SI nuclear response as

$$F_{\mathcal{N}}^{\mathrm{tot}}(E_R) = \sum_{N,N'=p,n} F_{1,1}^{(N,N')}(E_R, \mathcal{N}). \tag{17}$$

Here, since $\lambda_{\mathrm{SI}}^p = \lambda_{\mathrm{SI}}^n$, the total nuclear response reduces to the square of the customary Helm form factor [33] multiplied by the coherent enhancement of the cross section $A_{\mathcal{N}}^2$. In particular it reads $F_{\mathcal{N}}^{\mathrm{tot}}(E_R) = A_{\mathcal{N}}^2 F_{\mathrm{Helm}}^2(E_R)$. The function $\mathcal{I}(E_R) = \int_{v_{\mathrm{min}}}^{v_{\mathrm{esc}}} \mathrm{d}^3 v f_G(\vec{v} + \vec{v}_E(t))/v$ is instead the velocity integral encountered many times in the literature. It is worth noticing that $\mathcal{I}(E_R)$ can be written in this way because in the "standard" SI interaction the operator that the describes the nonrelativistic limit of the effective Lagrangian does not carry any dependences on the relative velocity $\vec{v}$. In Section 3.2 the interpretation of the experimental results in terms of the "standard" SI interaction is briefly reviewed.

2.3. Experimental Observables. Since, as already stated, the Earth's orbital velocity projected in the galactic plane is relatively small compared to the drift velocity of the Sun, we can then expand the recoil rate (11), assuming that the velocity distribution is not strongly anisotropic. Then, by means then of (7), one gets

$$\frac{\mathrm{d}R_{\mathcal{N}}}{\mathrm{d}E_R}(t) \simeq \left.\frac{\mathrm{d}R_{\mathcal{N}}}{\mathrm{d}E_R}\right|_{v_E=v_\odot} + \frac{\partial}{\partial v_E}\left.\frac{\mathrm{d}R_{\mathcal{N}}}{\mathrm{d}E_R}\right|_{v_E=v_\odot} \Delta v \cos\left[\frac{2\pi(t-\phi)}{\tau}\right]. \tag{18}$$

In order now to properly reproduce the experimental rate of nuclear recoil and in turn the expected number of events in a certain energy bin, one should take into account the response of the detectors as well. It can be done by the following energy convolution and transformation:

$$\frac{\mathrm{d}R}{\mathrm{d}E'} = \sum_{\mathcal{N}} \epsilon(E') \int_0^\infty \mathrm{d}E_R \mathcal{K}_{\mathcal{N}}(q_{\mathcal{N}} E_R, E') \frac{\mathrm{d}R_{\mathcal{N}}}{\mathrm{d}E_R}(E_R), \tag{19}$$

where E' is the detected energy and the functions $\mathcal{K}_{\mathcal{N}}(q_{\mathcal{N}} E_R, E')$ and $\epsilon(E')$ are the energy resolution centered in $q_{\mathcal{N}} E_R$ and the detector's efficiency, respectively. Here the sum runs over the different species of the detectors (e.g., DAMA is a multiple target experiment composed by crystal of sodium and iodine) and $q_{\mathcal{N}}$ is the so-called

quenching factor that takes account of the partial recollection of the released energy in the detector. After convolving with all the experimental effects, (19) must be averaged over the energy bins of the detector. For each energy bin k, we then obtain the number of the unmodulated events $N_{0\,k}^{\mathrm{th}}$ and of the modulated ones $N_{m\,k}^{\mathrm{th}}$ as

$$N_{0\,k}^{\mathrm{th}} = w_k \int_{\Delta E_k} \mathrm{d}E' \left.\frac{\mathrm{d}R}{\mathrm{d}E'}\right|_{v_E=v_\odot}, \tag{20}$$

$$N_{m\,k}^{\mathrm{th}} = w_k \Delta v \int_{\Delta E_k} \mathrm{d}E' \left.\frac{\partial}{\partial v_E}\frac{\mathrm{d}R}{\mathrm{d}E'}\right|_{v_E=v_\odot}, \tag{21}$$

where w_k is the exposure (expressed kilograms per day) and ΔE_k is the width of the kth-esime energy bin. $N_{0\,k}^{\mathrm{th}}$ and $N_{m\,k}^{\mathrm{th}}$ are the relevant quantities that one can use for the analysis of the experiments which address the annual modulation effect, namely, DAMA and CoGeNT. For the other experiments, only $N_{0\,k}^{\mathrm{th}}$ is instead relevant.

Collecting all the elements in the previous equations we expand (20) and (21) and write

$$\begin{aligned} N_{0\,k}^{\mathrm{th}} &= X \sum_{i,j=1}^{16} \sum_{N,N'=p,n} \mathfrak{c}_i^N\left(\lambda, m_\chi\right) \mathfrak{c}_j^{N'}\left(\lambda, m_\chi\right) \\ &\quad \times \widetilde{\mathscr{F}}_{i,j}^{(N,N')}\left(m_\chi, k\right)\Big|_{v_E=v_\odot}, \\ N_{m\,k}^{\mathrm{th}} &= X\Delta v \sum_{i,j=1}^{16} \sum_{N,N'=p,n} \mathfrak{c}_i^N\left(\lambda, m_\chi\right) \mathfrak{c}_j^{N'}\left(\lambda, m_\chi\right) \frac{\partial}{\partial v_E} \\ &\quad \times \widetilde{\mathscr{F}}_{i,j}^{(N,N')}\left(m_\chi, k\right)\Big|_{v_E=v_\odot}. \end{aligned} \tag{22}$$

Here $\widetilde{\mathscr{F}}_{i,j}^{(N,N')}(m_\chi, k)$ is a sort of *integrated form factor* that encapsulates all the information related to nuclear physics, astrophysics, and the detector dependency of the rate. There is one of these factors for each energy bin k of each experiment under consideration and for each choice of the operators pair (i, j) and nucleons pair (N, N'). It reads explicitly

$$\begin{aligned} &\widetilde{\mathscr{F}}_{i,j}^{(N,N')}\left(m_\chi, k\right) \\ &\quad = w_k \sum_{\mathscr{N}} \xi_{\mathscr{N}} \int_{\Delta E_k} \mathrm{d}E' \epsilon\left(E'\right) \\ &\qquad \times \int_0^\infty \mathrm{d}E_R \mathscr{K}_T\left(q_{\mathscr{N}} E_R, E'\right) \\ &\qquad\quad \times \mathscr{F}_{i,j}^{(N,N')}\left(E_R, \mathscr{N}\right). \end{aligned} \tag{23}$$

It is worth noticing that the linearity of the expected number of events in the *integrated form factors* is a fundamental ingredient. This, indeed, lets us parametrize the model dependent part of the rate from the model independent one, encapsulated in the function $\widetilde{\mathscr{F}}_{i,j}^{(N,N')}(m_\chi, k)$. Therefore, if the experimental collaborations, instead of presenting the experimental results in terms of a specific DM model, release all of this finite number of *integrated form factors*, one will be easily able to obtain the expected number of events for any kind of interactions, whose particle physics is completely encapsulated in the coefficient $\mathfrak{c}_i^N$. A first example of the potentiality of such parametrization has been presented in [32]. In particular the authors provide a self-contained set of numerical tools based on the *integrated form factors* above, to derive the bounds from some current direct detection experiments on virtually any arbitrary model of DM elastically scattering on target nuclei.

3. Direct Detection Status

3.1. Experimental Landscape. The elusive nature of DM particles makes their detection a challenge for experimentalist: in fact, considering typical atomic masses for the target nuclei of $m_{\mathscr{N}} = 100\,\mathrm{GeV}$ and typical properties for the DM halo (Maxwell-Boltzmann distribution with dispersion velocity $v_0 = 220\,\mathrm{km/s}$), DM particles should induce tiny nuclear recoil in the range $1 \div 10^3\,\mathrm{keV}$ with a total rate lower than 1 cpd/kg/keV (here cpd refers to counts per days). Due to this rare phenomenon, the experimental priorities in this field are as follows:

(i) the detectors must work deeply underground in order to avoid the high rate interaction induced by cosmic rays scattering off on target nuclei,

(ii) they must use active shields and very clean materials against the residual radioactivity in the tunnel (mostly α-particles, neutrons, and photons),

(iii) they must distinguish multiple scattering, simply because DM particles do not interact twice in the detector, being of course weakly interacting particles.

A variety of different experimental techniques with the aim of measuring the tiny energy released by a DM interaction have been developed. In the following the main channels by which the scattered nucleus can deposit energy in the detectors are summarized as follows.

(i) *Scintillation detection:* a particle interacting within a scintillating target induces the emission of light produced by the deexcitation of exited atoms. This light can be detected by appropriate photomultipliers. Typically NaI(Tl) and xenon are used as scintillators.

(ii) *Ionization detection:* a particle interacting inside a target produces an amount of free electron-ion pairs that can be detected with a collecting drift field and a device sensitive to the electric charge.

(iii) *Phonon detection:* a particle interacting inside a detector releases a tiny energy deposition with a subsequently increase of the temperature. Cryogenic apparatus working at very low temperature (around few mK) are able to measure this small variation making this detection technique possible.

Since various types of interacting particles release a different amount of energy in the channels commented upon above, for a better rejection of the background events, most

of the experiments are designed to be sensitive to more than one of them. Indeed, thanks to this ability, the ratio between two channels can be used to distinguish between nuclear (due to a DM interaction) and electromagnetic recoils.

The only two experiments that do not use this kind of experimental technique are DAMA and CoGeNT that, perhaps not coincidentally, were the only two detectors (until the CRESST-II and recently the CDMS-Si results) observing an excess in their counting rate. In particular, since both the experiments are not able to disentangle the nuclear recoil signals from the electromagnetic ones, they infer the presence of DM in our halo by exploiting the model independent annual modulation signature in the counting rate. As follows, I review the most important experiments in this field.

3.1.1. DAMA. The DAMA experiment, located at the National Laboratory of Gran Sasso, is an observatory for rare processes made of highly radiopure scintillators (NaI(Tl) crystals). In particular the former DAMA/NaI and the current DAMA/Libra experiments have the main aim of investigating the presence of DM particles in the galactic halo by exploiting the model independent annual modulation induced by a DM interaction.

The DAMA detector is only able to measure the fraction of energy deposited in scintillation light, while the phonon excitation due to multiple nuclear interactions is not detected. This effect, as commented upon in Section 2.3, is taken into account by the so-called quenching factor. In particular, for NaI(Tl) crystals, one normally considers $q_{\mathrm{Na}} \simeq 0.3$ and $q_{\mathrm{I}} \simeq 0.09$ [34]. It is, however, known [34–36] that some scattered nuclei can travel long distances along the crystallographic axes and planes without colliding with other nuclei. This process is called channeling effect, and since no phonon excitation is produced, the scattered nuclei deposit all the energy in the detector electromagnetically ($q_{\mathcal{N}} \simeq 1$). The fraction of channeling depends on the nucleus itself, on the recoil energy and strongly on the temperature. It has been calculated, for instance, in [35] and, in particular, it has been found that, for low energy recoiling Na and I ions, the fraction of channeled events can be relatively large. Nevertheless, this result has not been confirmed by other theoretical [37–39] and experimental studies [40], which instead suggest that the channeling effect in NaI crystals is negligible.

The DAMA collaboration published results of the combined DAMA/NaI and DAMA/Libra experiments [41, 42], corresponding to an exposure of 1.17 ton·yr for a target. They observed a cosine-like modulation, present only in the *single-hit* events, with a measured period $\tau = (0.999 \pm 0.002)$ yr and a phase $t' = (146 \pm 7)$ days well compatible with the roughly 152.30 days expected for DM signals (see the previous section). The modulation is present only in the low energy window (2–6) keVee (here, keVee refers to electron equivalent recoil energy. This must be converted with the quenching factor in order to get the total energy released to the nucleus by the scattering process (E_R [keV] $\equiv E_R$ [keVee]$/q_{\mathcal{N}}$)) and its amplitude $N^{\mathrm{exp}}_{m\,(2-6)}$ is equal to (0.0116 ± 0.0013) cpd/(kg·keV) at 8.9σ CL [42].

3.1.2. CoGeNT. The CoGeNT experiment employs p-type point-contact Germanium detectors operating in the Soudan Underground Laboratory.

Like DAMA, the experiment performs just one of the techniques commented upon above; namely, the p-type point-contact germanium detectors only measure the fraction of energy deposited by incident particles in the form of ionization. The lack of energy measured is again taken into account by the quenching factor that can be extracted through the following empirical relation $E_{\mathrm{det}} = 0.2E_R^{1,12}$ [43]. By virtue of its low energy threshold (0.4 keVee) and the ability to reject surface backgrounds, this type of detector is particularly sensitive to light DM candidates, although large background contamination may be present for these low energies.

In 2010 the collaboration has reported a step rise of nuclear recoil spectrum at low energy which is not directly explainable in terms of known radioactive background [44]. The energy region probed by CoGeNT partially overlaps with the one in which the DAMA apparatus reported the annual modulation signal, and therefore it is natural to interpret the excess at low energy due to a DM interaction. In view of that, fifteen months of cumulative CoGeNT data (442 live days) have been also examined in order to look for an annual modulation signature [45]. In particular the CoGeNT data seem to favor a cosine-like modulation slightly shifted in phase with respect to the one measured by DAMA. The modulation is again only present at low energy with a statistical significance of 2.8σ CL, limited by the short exposure.

Very recently, the collaboration presented a 3.4-year data taking, with an improved analysis that allows a better discrimination between pure bulk and pure surface events [46, 47]. In the same energy region, where in 2010 they observed a step rise of the nuclear recoil spectrum, they still reported a preference for an annual modulation in the pure bulk counting rate. Although the statistical significance of the modulation is modest (2.2σ CL), the phase is compatible with the one observed by DAMA.

3.1.3. CRESST-II. The CRESST-II cryogenic dark matter experiment, located at the national laboratory of Gran Sasso, employs 300 g of scintillating $CaWO_4$ crystals.

In particular the eight moduli of the experiments measure the deposited energy in the form of phonons and scintillation light. The former provides a precise measure of the energy deposited, while the ratio between them gives an excellent rejection of the background events.

In 2011 the collaboration completed a 730 kg·day data taking [48]. In particular, 67 events were found in the DM acceptance region with an expected background contributions in the same band which is not sufficient to explain all the observed events. The resulting statistical significance, at which the background-only hypothesis is rejected, is roughly 4.5σ CL.

3.1.4. CDMS. The CDMS experiment, located at the Soudan Underground Laboratory, is composed by germanium and silicon cryogenic detectors.

In particular 19 germanium and 11 silicon detectors measure the deposited energy in the form of phonons and ionization through superconducting technology. Thanks to the ability of detecting these two signals, the rejection of the electromagnetic recoils can be obtained by the ratio among them.

In 2009 the CDMS collaboration [49] has reported no significant evidence for DM interaction. In particular, only germanium detectors were used with an exposure of 612 kg·days. The collaboration observed two events in the signal region with energy 12.3 keVnr and 15.5 keVnr (here, keVnr refers to nuclear recoil energy. Unlike the electron equivalent recoil energy, it already represents the total energy released to the nucleus by the scattering process (E_R [keV] ≡ E_R [keVnr])), against an expected background of radiogenic neutrons, cosmogenic neutrons, and misidentified surface events equal to roughly 0.9 events.

More recently, the collaboration has also presented results based on the silicon analysis [50, 51]. In [51], a blind analysis of 140.2 kg·days revealed three DM candidate events in the signal region with an expected background of roughly 0.62 events. A profile likelihood ratio statistical test of the three events yields a 0.19% probability when the known-background-only hypothesis is tested, against the alternative DM + background hypothesis.

3.1.5. Xenon Experiments. Direct detection experiments based on liquid/gaseous xenon have done stunning progresses in the last decade. Indeed, thanks to the advantage in scale ability and to the good reconstruction of the three-dimensional coordinates, these experiments are among the largest in terms of fiducial mass.

Discrimination between nuclear and electromagnetic recoils is achieved by the ratio between the scintillation signal due to a particle interaction in the liquid xenon and the subsequent ionization signal in the gas phase of the detector. Furthermore, the large mass number of the xenon nuclei makes them an excellent target for the detection of DM particles with SI interaction. However, the experiments based on liquid xenon are also sensitive to the *n*-DM spin dependent interaction, by virtue of the unpaired neutron of the ^{129}Xe and ^{131}Xe isotopes.

In the following the results of the main experiments using the double-phase xenon technology are summarized.

(i) *XENON experiment:* the XENON detector is a two-phase time projection chamber located at the national laboratory of Gran Sasso. The first stage of the experiment was installed underground during March 2006, and it searched for DM interactions until October 2007. In 2008 the collaboration reported a blind analysis with an exposure of 5.4 × 58.6 kg·days, which yields no significance evidence for DM interactions [52].

More recently the XENON10 experiment has been superseded by XENON100 with more than one order of magnitude improvement in sensitivity. In [53], the collaboration reported the results of the last run, a blind analysis with an exposure of 34 × 224.6 kg·days which again yielded no evidence for DM interactions. In particular, the two observed events in the predefined nuclear recoil energy range of 6.6–43.3 keVnr were consistent with the background expectation of roughly 1 event.

(iii) *LUX experiment:* the LUX experiment is a dual-phase xenon time-projection chamber operated at the Sanford Underground Research Facility in South Dakota. Like the XENON100 experiment, it measures both the scintillation light and the ionization in the gas phase to disentangle the nuclear recoils from the electromagnetic ones. In [54], a nonblind analysis was performed on data, collected with an exposure of 118.3 × 85.3 kg·days. After cuts, 160 events were found within the signal energy region. The collaboration found that all of these events are compatible with the expected electron recoil background.

3.1.6. COUPP. The COUPP experiment operating at SNOLAB in Ontario is a 4 kg CF_3I bubble chamber. By virtue of its unpaired proton, the fluorine nucleus gives an excellent sensitivity for *p*-DM spin-dependent interactions, while the iodine enhances the sensitivity for the SI ones.

Particles entering the liquid in the superheated phase create an ionization tracks, around which the liquid vaporizes, forming microscopic bubbles. Bubbles grow in size as the chamber expands, making the detector able to record them both photographically and by pressure and acoustic measurements. The discrimination between nuclear and electromagnetic recoils can be achieved by choosing an appropriate chamber pressure and temperature. Indeed, under this condition, the abundant gamma-ray and beta-decay backgrounds do not nucleate bubbles.

In [55], data obtained for an effective exposure to single recoil events of 437.4 kg·days (taking into account the 79.1% detection efficiency) were presented. Twenty single nuclear recoil events passing all the analysis cuts were observed over the three energy bins. Due to uncertainties in the neutron background estimation, the collaboration has not attempted any background subtraction and instead has treated all of them as DM events.

3.2. Interpretation in Terms of the "Standard" SI Interaction. There are many studies in literature that try to analyze the implications of the results of DAMA and the anomalies in CoGeNT and CRESST-II and recently in CDMS-Si together with the null results from other experiments in terms of specific DM models and interactions. A routine way to compare results from different DM experiments is by assuming a particular DM velocity distribution and a certain type of DM-nucleus interaction. The customary choices that can often be found in literature are (i) a truncated Maxwell-Boltzmann velocity distribution with isotropic velocity dispersion $v_0 = 220$ km/s and (ii) DM particles coupling through a contact SI interaction with equal strength to the protons and neutrons. In this case one customarily chooses the total DM-nucleon cross section σ_{SI}

defined in Section 2.2.1 together with the DM mass m_χ as free parameters, since the bounds and the allowed regions from different experiments can be compared on the same plot.

In Figure 2 a compilation of the allowed regions of the positive results experiments and the constraints coming from null results taken from different experimental collaborations are shown. Without entering in the details of the different analysis, we summarize the interpretation of the datasets of the positive results experiments listed above in terms of the "standard" SI contact interaction as follows.

(i) The DAMA modulation signal effect has been shown to be compatible with two areas in the $(m_\chi, \sigma_{\rm SI})$ parameter space, due to the different kinematics experienced by the two targets in the scintillator. In particular, a region pointing towards DM masses in the 10 GeV ballpark and towards a cross section $\sigma_{\rm SI} \simeq 2 \times 10^{-40}$ cm^2 can be associated with a DM particle scattering off with sodium (see, e.g., the red contour in the top left-handed plot of Figure 2 denoted by DAMA/Na). Another region around DM masses of roughly 60 GeV is instead due to the scattering with the iodine. In this case the cross section is enhanced by a larger coherent factor and indeed the favored value is $\sigma_{\rm SI} \simeq 10^{-41}$ cm^2 (red contour denoted by DAMA/I).

(ii) The modulation in CoGeNT is mostly concentrated in the first two energy bins, close to the lower threshold of the detector. If this anomaly is interpreted in terms of SI contact interaction, it will be fitted by light DM candidates (around 9 GeV) with a total SI cross section $\sigma_{\rm SI} \simeq 3 \times 10^{-41}$ cm^2 (see, e.g., the red contour in the top right-handed plot of Figure 2).

(iii) Like DAMA, the CRESST-II experiment is a multiple target detector and therefore more than one allowed region is in general expected. In particular, as one can see in Figure 2, the region pointing towards light DM masses (around 12 GeV) and $\sigma_{\rm SI} \simeq 5 \times 10^{-41}$ cm^2 is due to the scattering with oxygen and calcium. On the other hand, the one pointing towards heavier DM mass (around 30 GeV) and cross section $\sigma_{\rm SI} \simeq 10^{-42}$ cm^2 can be associated with a DM particle scattering off with tungstenum. These regions are, for instance, denoted as gray contours in the top left-handed plot of Figure 2.

(iv) Very recently, also the 11 silicon detectors of the CDMS experiment reported an excess in their counting rate. Again, if the anomaly is interpreted in terms of SI contact interaction, it will be fitted by light DM particles (around 9 GeV) with a SI total cross section $\sigma_{\rm SI} \simeq 2 \times 10^{-41}$ cm^2 (blue regions in the bottom left-handed plot of Figure 2).

The interesting feature is that all the experiments employing light target nuclei seem to be compatible with a DM interpretation, which, for the "standard" SI contact interaction, pin-points the properties of the DM particle quite precisely; namely, it leads to DM masses in the 10 GeV ballpark and total cross section in the range (2×10^{-41} cm^2–2×10^{-40} cm^2).

On the other hand, the constraints coming from null results are very stringent, and in particular the XENON100 and recently the LUX results severely exclude the allowed parameter space of the positive results experiments. On a more specific level, before LUX, the XENON100 experiment provided the most stringent constraints for a DM mass above roughly 8 GeV, with a minimum of $\sigma_{\rm SI} \simeq 1.8 \times 10^{-44}$ cm^2 (see, e.g., the thick blue line in the top left-handed plot of Figure 2). Nowadays this bound has been beat out by the one of LUX by a factor ~2.5 (see the blue line in the bottom right-handed plot of Figure 2). Other relevant analyses can be found in [56–68].

3.3. Uncertainties. Nevertheless, since the actual range of masses and cross section critically depends on several assumptions, one always bears in mind all the uncertainties that enter in this field when interpreting the data in terms of a specific DM interaction.

(i) A first class of uncertainties comes from the poor knowledge of the properties of the DM halo. The often used Maxwell-Boltzmann halo with isotropic velocity dispersion is only a benchmark choice, not the physical description of it. Other possible choices (spherical halo with nonisotropic velocity dispersion, axisymmetric halo, triaxial halo, and the possibility to have corotating halo with different number densities) must be taken into account, in order to have a much better idea of how the velocity distribution affects the final results. In particular, it has been recently demonstrated that the uncertainties on the astrophysical part of the rate can be removed by comparing different experimental results in the $v_{\rm min}$ space (see, e.g., [69–77]). In this way one can, for instance, relax a bit the tension between the positive results and the constraints showed in Figure 2 up. However, this is not still sufficient to reconcile the complicated puzzle the experimental data have left to us (see, e.g., [77–80]).

(ii) A second class of uncertainties comes from the experimental side. For instance, the direct measurements of quenching factor are performed with reference detectors, and thus the systematic uncertainties, important for all the detectors in direct DM searches, could be larger than what we normally assumed. These must be carefully investigated, because they produce a significant shift of the allowed regions in the total cross section/DM mass plane.

(iii) Together with these main uncertainties, the third and perhaps the most important class of them comes from the nature of the DM interaction and in turn from the nuclear responses of the target nuclei. Most of the models tested in recent years are based on the assumption that the mechanism of interaction is realized through a contact interaction. Deviations from this standard phenomenological approach are interesting to study, since, from more general conditions, the DM parameter space can be analyzed.

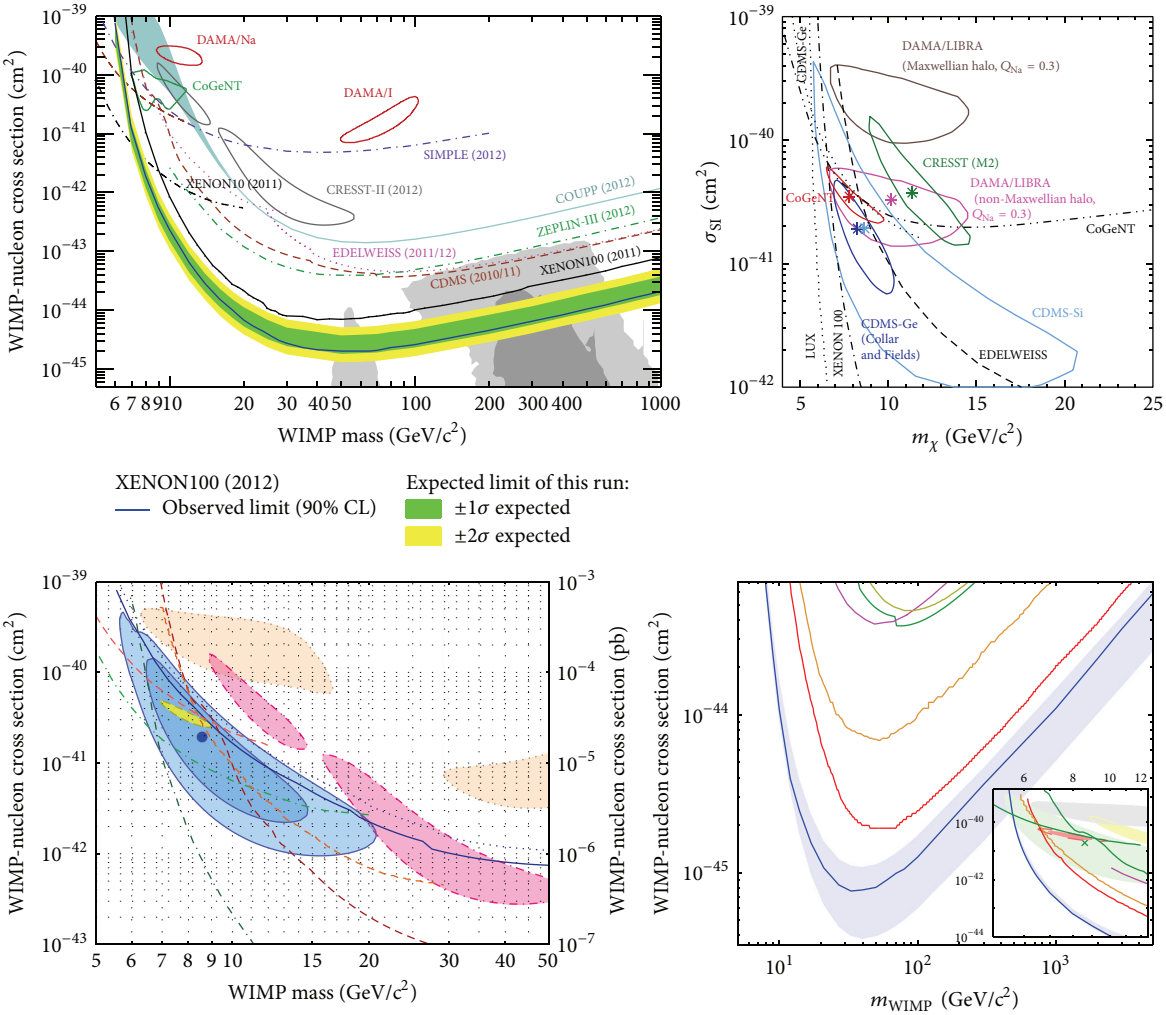

FIGURE 2: *A compilation of the allowed regions and the constraints* for the "standard" SI contact interaction in the (m_χ, σ_{SI}) plane. The plots on the top row are taken from [53] (left) and from [46] (right), while those in the bottom row are taken from [51] (left) and from [54] (right). The galactic halo has been assumed in the form of an isothermal sphere with velocity dispersion $v_0 = 220$ km/s and local DM energy density $\rho_\odot = 0.3$ GeV/cm^3.

In particular, there is a concrete possibility to remove the uncertainties coming from the nature of interaction thanks to the formalism of nonrelativistic operator reviewed in Section 2.2. On a more specific level, if the experimental collaborations, in addition to presenting the results in terms of a specific DM-nucleus interaction, also provide all the model independent *integrated form factors*, it will be extremely useful for the community. Indeed, in this way one can easily compute the expected number of events for any kind of interactions (e.g., including isospin violating interactions, momentum-dependent form factors, and velocity dependent form factors) and compare it directly with the experimental results.

Therefore the data must be treated very prudently with a maximally conservative attitude, simply because slightly modification of the assumptions summarized above can affect the theoretical interpretation of the experimental results in a relevant way. In the next section, I will focus on the uncertainties coming from the nature of interaction and in particular I am going to show how the allowed regions and constraints are modified, if an exchanged momentum dependent DM-nucleus interaction is taken into account.

4. Long Range Interaction

So far, the LHC has not reported any evidences of physics beyond the standard model. An optimistic point of view is that the new physics threshold is truly around the corner. A pessimistic and maybe more realistic point of view is that the LHC results are instead telling us that the TeV scale is not a fundamental energy scale for new physics and therefore all the new theories beyond the standard model are, let us say, unnatural. Within this picture there is not any particular reason to expect new particles in the TeV mass range weakly interacting with ordinary matter. Therefore it

should be time to ask ourselves whether there are other indications of the relevant energy scale. DM may play a central role in this picture. Indeed, the closeness between Ω_χ and Ω_b, usually referred to as a cosmic coincidence problem, might suggest a profound similarity between the dark and the ordinary sectors. Indeed, both ρ_χ and ρ_b scale as $1/a^3$ with the expansion of the Universe, and their ratio is independent of time. Why these two fractions are then comparable, if the ordinary and the dark sectors have a drastically different nature and different origin? A hidden parallel sector (mirror world (the idea of a mirror world was suggested before the advent of the standard model (see, e.g., [81, 82]). The idea that the mirror particles might constitute the DM of the Universe was instead discussed in [83, 84])) may shed light on this cosmic coincident problem [85]. Indeed, it is tantalizing to imagine that the dark world could be similarly complex (CP violating and asymmetric), full of forces (e.g., dark electromagnetism), and matter (dominant constituent with a mass around few GeV) that are invisible to us. For a review of mirror dark world; see, for example, [86, 87].

To be more concrete the phenomenology of a complex dark sector, in which the matter fields are charged under an extra $U(1)$ gauge group, is particularly interesting. In this case, the physics of the dark sector in itself can be as complicated as the one of our sector, providing at the same time also a feeble interaction between the two worlds. Indeed, thanks to the following renormalizable Lagrangian:

$$\mathscr{L} = \frac{\epsilon_\phi}{2} F^{\mu\nu} F'_{\mu\nu}, \tag{24}$$

the new $U(1)$ gauge boson ϕ may possess a small kinetic mixing ϵ_ϕ with the ordinary photon. Here $F_{\mu\nu}$ and $F'_{\mu\nu}$ are the field strength tensors of the ordinary and "dark" electromagnetism, respectively. One effect of this mixing is to cause DM particles to couple with ordinary particles with effective millicharge $\epsilon_\phi e$ [88–90], and therefore a Rutherford-like interaction gives rise if the mass of the new $U(1)$ gauge boson is smaller than the typical exchanged momentum in the interaction.

4.1. Derivation of the Main Equations. Apart from the theoretical motivations which are interesting and quite strong, what describes in the nonrelativistic limit the scattering between millicharged DM particles and the protons (notice that the interaction here maximally violates the isospin; e.g., the DM-neutron coupling is zero) is the following Yukawa potential:

$$V(r) = \frac{\epsilon_\phi}{4\pi} \frac{e e_\chi}{r} e^{-m_\phi r}, \tag{25}$$

where $\epsilon_\phi e$ is the effective millicharge of the protons inside the nucleus felt by a DM particle with "dark" charge e_χ. Here m_ϕ is the mass of the dark photon that acts like an electronic cloud which screens the charges of the particles involved in the scattering. The DM-proton matrix element can be then obtained by performing the Fourier transform of (25) which writes

$$\begin{aligned} \mathscr{M}_p &= 4\, m_p m_\chi \int_0^\infty \mathrm{d}r\, 2\pi r^2 \int_{-1}^{+1} \mathrm{d}\, \cos\theta e^{-iqr\cos\theta} V(r) \\ &= \mathfrak{c}_Y^p \left(q^2\right) \mathcal{O}_1^{\mathrm{NR}}, \end{aligned} \tag{26}$$

where $q = (2m_\mathcal{N} E_R)^{1/2}$ is the exchanged momentum, θ is the scatter angle in the centre-of-mass frame, and $\mathfrak{c}_Y^p(q^2) = 4\epsilon_\phi e e_\chi m_p m_\chi/(q^2 + m_\phi^2)$. Since $\mathcal{O}_1^{\mathrm{NR}} = \mathbb{1}$, the interaction, as already mentioned in Section 2.2, is SI like the usual case but with a coefficient which is instead dependent on the exchanged momentum in the scattering. Summing now over the total number of protons in the nucleus $Z_\mathcal{N}$ and, if the dark sector is made of stable composite particles, over the total number of charge elementary constituents Z_χ, the square of the DM-nucleus matrix element reads

$$\overline{|\mathscr{M}_\mathcal{N}|^2} = 16 m_\mathcal{N}^2 m_\chi^2 \left(\frac{\epsilon_\phi Z_\mathcal{N} e Z_\chi e_\chi}{q^2 + m_\phi^2} \right)^2 F_{\mathrm{Helm}}^2 \left(q^2\right), \tag{27}$$

where $F_{\mathrm{Helm}}^2(q^2)$ is the usual Helm form factor. Notice that in general this equation should be also multiplied for the form factor of the composite DM particle. For our computation we assume it to be equal to one. Plugging back the DM-nucleus matrix element in (8) the differential cross section will be

$$\frac{\mathrm{d}\sigma_\mathcal{N}}{\mathrm{d}E_R} = \frac{8\pi m_\mathcal{N}}{v^2} \epsilon_\phi^2 \alpha^2 k_\chi^2 \left(\frac{1}{q^2 + m_\phi^2} \right)^2 Z_\mathcal{N}^2 F_{\mathrm{Helm}}^2 \left(q^2\right), \tag{28}$$

where $\alpha = e^2/4\pi$ is the electromagnetic fine structure constant and $k_\chi = Z_\chi e_\chi/e$ is a factor that measures the strength of the DM-dark photon coupling.

In order to have a rough comparison with the "standard" picture (SI contact interaction), the differential rate of nuclear recoil can be cast in the following form:

$$\begin{aligned} \frac{\mathrm{d}R_\mathcal{N}}{\mathrm{d}E_R} = \frac{\xi_\mathcal{N}}{m_\mathcal{N}} \frac{\rho_\odot}{m_\chi} \left[\frac{m_\mathcal{N}}{2\mu_N^2} A_\mathcal{N}^2 \sigma_{\phi\gamma}^p \mathcal{J}\left(E_R\right) F_{\mathrm{Helm}}^2 \left(E_R\right) \right] \\ \times \mathcal{G}\left(E_R\right), \end{aligned} \tag{29}$$

where

$$\begin{aligned} \sigma_{\phi\gamma}^p &= \frac{16\pi\alpha^2 \epsilon_\phi^2 k_\chi^2}{m_N^4} \mu_N^2 \\ &\simeq \left(\frac{\epsilon_\phi}{10^{-5}} \right)^2 \left(\frac{k_\chi}{1} \right)^2 \left(\frac{\mu_N}{1\,\mathrm{GeV}} \right)^2 10^{-40}\,\mathrm{cm}^2 \end{aligned} \tag{30}$$

is a normalized total cross section that encapsulates all the dependences on the dark sector vertex and the kinetic mixing parameter, and the function

$$\mathcal{G}\left(E_R\right) = \frac{Z_\mathcal{N}^2}{A_\mathcal{N}^2} \left[\frac{m_N^2}{q^2 + m_\phi^2} \right]^2 = \frac{Z_\mathcal{N}^2}{A_\mathcal{N}^2} \left[\frac{m_N^2}{2m_\mathcal{N} E_R + m_\phi^2} \right]^2 \tag{31}$$

measures the deviation of the allowed regions and constraints compared to the "standard" SI contact cross section. Here the function $\mathcal{G}(E_R)$ is a sort of DM form factors which clearly exhibits two limits.

(i) Point-like limit ($q \ll m_\phi$): in this regime $\mathcal{G}(E_R) = (Z_\mathcal{N}/A_\mathcal{N})^2 m_N^4/m_\phi^4$ is independent of E_R and therefore the interaction is of a contact type. Indeed, the rate of nuclear recoil turns out to be proportional to $\alpha^2\epsilon_\phi^2 k_\chi^2/m_\phi^4$, which plays the same role of the Fermi's constant in weak interaction. The factor $(Z_\mathcal{N}/A_\mathcal{N})^2$ shows up the fact that millicharged DM particles only couple with protons. Therefore, it is expected that the allowed regions and bounds in the plane $(m_\chi, \sigma_{\phi\gamma}^p)$ will be rigid shifted of a factor ~4 up with respect to the "standard" SI scenario, in which a DM particle symmetrically couples both with neutrons and protons.

(ii) Long range limit ($q \gg m_\phi$): in this regime $\mathcal{G}(E_R) = (Z_\mathcal{N}/A_\mathcal{N})^2 m_N^4/(4m_\mathcal{N}^2 E_R^2)$ and therefore the differential cross section acquires an explicit dependence on the nuclear recoil energy, and a Rutherford-like cross section gives rise ($\mathrm{d}\sigma_\mathcal{N}/\mathrm{d}E_R \propto 1/q^4$). Experiments with low energy thresholds and light target nuclei (e.g., DAMA and CoGeNT) are therefore more sensitive than the ones with high thresholds and heavy targets (e.g., XENON100). The compatibility among the experiments could therefore be improved.

Considering typical nuclei ($m_\mathcal{N} \sim 100$ GeV) and recoil energies (few keV) in the range of interest of the current experiments, the transition between the two limits is obtained for $m_\phi \sim \mathcal{O}(10)$ MeV. Since $q^2 \propto m_\mathcal{N}$, increasing $m_\mathcal{N}$ the transition occurs at lower m_ϕ. Notice that once the long range regime is reached ($m_\phi \lesssim 10$ MeV), the differential cross section is independent of the mass of the mediator.

4.2. Results. In our analysis we consider as free parameters the normalized total cross section $\sigma_{\phi\gamma}^p$, the mass of the dark photon m_ϕ, and of course one of the DM particle m_χ. The velocity distribution has been assumed to be Maxwell-Boltzmann-like with a velocity dispersion $v_0 = 220$ km/s. For the local DM density we have chosen $\rho_\odot = 0.3\,\mathrm{GeV/cm^3}$. For all the positive results experiments we use a different technique for analyzing the datasets with respect to the one often found in literature. Specifically, we adopt the same approach of [91], in which the null hypothesis is tested. From this kind of statistical test we can then extract the level at which the absence of signal on top of the background in CRESST-II and the absence of modulation in DAMA and CoGeNT is rejected.

In Figure 3 the allowed regions of the positive results experiments and constraints coming from null results in the plane $(m_\chi, \sigma_{\phi\gamma}^p)$ are shown. For a better visualization of the transition from the contact to the long range regime, we have fixed three values of the dark photon mass; namely, $m_\phi = 1$ GeV (left plot corresponding to the contact limit), $m_\phi = 30$ MeV (central plot), and $m_\phi = 0$ (right plot corresponding to the pure long range regime). In all plots the solid green contours individuate the regions compatible with the DAMA annual modulation [41, 42], without considering the channeling effect. The short-dashed blue contour refers to the region derived from the CoGeNT annual modulation signal data published in [45] (in [46, 47] the collaboration reanalyzed the data finding that the background of surface events was underestimated. In view of that we expect that the CoGeNT allowed regions in the $(m_\chi, \sigma_{\phi\gamma}^p)$ plane will shrink around its best value, like the one reported for the "standard" SI contact interaction (see, e.g., the red contour in the top right-handed plot of Figure 2)). The dashed brown contours individuate the allowed regions compatible with the CRESST-II excess [48]. For each experiment the contour lines cover at least one area in the $(m_\chi, \sigma_{\phi\gamma}^p)$ plane. Specifically, they refer to regions where the absence of annual modulation can be rejected at 7σ CL (outer region) and 8σ CL (inner region) for DAMA, and 1σ CL for CoGeNT. For CRESST-II the absence of an excess is instead excluded at 3σ CL (outer region) and 4σ CL (inner region).

Very recently, also the 11 silicon detectors of the CDMS experiment have reported an excess in their counting rate. Since the results presented in Figure 3 are based on [24] published in 2011, we do not include a full statistical analysis of the CDMS-Si datasets. We attempt however an analytical comparison between the results arising from the interaction studied here and the standard SI contact picture (blue regions in the bottom left-handed plot of Figure 2). More precisely, defining $\langle\mathcal{G}\rangle \equiv \mathcal{G}(\langle E_R\rangle)$, where $\langle E_R\rangle \simeq 10$ keV is the average recoil energy of the three events observed [51], the CDMS-Si allowed region in the $(m_\chi, \sigma_{\mathrm{SI}})$ plane can be projected in the parameter space of Figure 3, through the relation $(m_\chi, \sigma_{\phi\gamma}^p) \equiv (m_\chi, \sigma_{\mathrm{SI}}/\langle\mathcal{G}\rangle)$. Recalling now that the best fit value of the SI cross section is $\sigma_{\mathrm{SI}}^{\mathrm{best}} \simeq 2\times10^{-41}\,\mathrm{cm^2}$, we expect that the CDMS-Si allowed region in the $(m_\chi, \sigma_{\phi\gamma}^p)$ plane will still point towards light DM candidate, but with a normalized total cross section $\sigma_{\phi\gamma}^p = A_{\mathrm{Si}}^2/Z_{\mathrm{Si}}^2 m_\phi^4/m_N^4\sigma_{\mathrm{SI}}^{\mathrm{best}} \simeq 10^{-40}\,\mathrm{cm^2}$ in the point-like regime ($m_\phi = 1$ GeV), and $\sigma_{\phi\gamma}^p = A_{\mathrm{Si}}^2/Z_{\mathrm{Si}}^2 4m_{\mathrm{Si}}^2\langle E_R\rangle^2/m_N^4\sigma_{\mathrm{SI}}^{\mathrm{best}} \simeq 3\times10^{-47}\,\mathrm{cm^2}$ in the long range one ($m_\phi = 0$).

Constraints, derived at 5σ CL, are shown as dashed gray lines for CDMS-Ge and magenta lines for XENON100. In particular, in order to bracket as much as possible the uncertainties coming from the poor knowledge of the detection efficiency close to the lower threshold; for the XENON100 bound, we adopt two approaches: (i) a case (dotted lines) in which the constraints are computed with the nominal value of the lower threshold of 4 PHE and of the effective luminosity [92], which is a sort of quenching factors in liquid xenon and (ii) another case (dashed lines) in which the constraints are computed by considering a higher threshold of 8 PHE: this is in order to determine a situation which is nearly independent of the poor knowledge of the effective luminosity (especially at very low nuclear recoil) and more important on the statistical distribution of the few PHE collected close to the threshold of the detector. For similar discussions; see [93, 94].

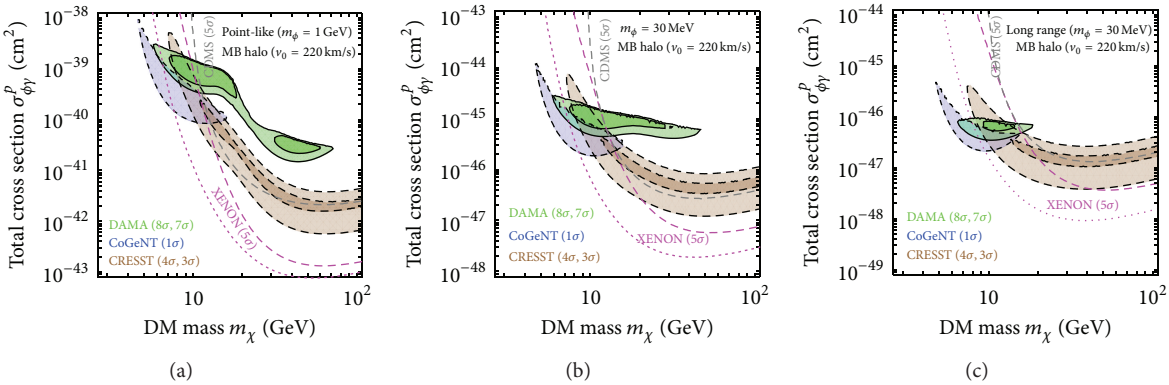

Figure 3: *Normalized total cross section as a function of the dark matter mass*. For a better visualization of the transition from the contact to the long range regime, we have fixed three values of the dark photon mass; namely, $m_\phi = 1$ GeV (a), $m_\phi = 30$ MeV (b), and $m_\phi = 0$ (c). In all plots we show the regions where the absence of annual modulation can be rejected at 7σ CL (outer region) and 8σ CL (inner region) for DAMA (solid green contours) and 1σ CL for CoGeNT (solid green contours). For CRESST-II (solid green contours) the absence of an excess is instead excluded at 3σ CL (outer region) and 4σ CL (inner region). Constraints, derived at 5σ CL, are shown as dashed gray lines for CDMS-Ge and magenta lines for XENON100. These results have been presented in [24, 25].

In October 2013, also the LUX collaboration announced their first DM search results. With the data collected in just 85 live-days, they were able to set the most stringent bound on the SI contact cross section, with respect to the preexisting limits. We do not perform a full statistical analysis of their data, since, as already pointed out, the results in Figure 3 are taken from [24]. Nevertheless, since both XENON and LUX are based on the same double-phase xenon technology, we can estimate the bound on $\sigma^p_{\phi\gamma}$, just by rescaling the magenta lines in Figure 3 with the exposures of the two experiments. Naively, we then expect that the LUX bound will be a factor $w_{\mathrm{LUX}}/w_{\mathrm{XENON100}} \simeq 1.5$ more stringent with respect to XENON100.

We can see, as expected from the discussion above, that the agreement among the positive results experiments increases moving towards long range interaction without being excluded by both the XENON100 and LUX bounds, if our conservative choice for the lower threshold is taken into account. In particular, a common region pointing towards a DM mass around 15 GeV with a normalized total cross section $\sigma^p_{\phi\gamma} \sim 10^{-46}$ cm^2 has been found. Since the normalized total cross section $\sigma^p_{\phi\gamma}$ depends collectively on the kinetic mixing parameter ϵ_ϕ and on the DM-dark photon coupling encoded in the parameter k_χ (see (30)), keeping fixed, for instance, two values of k_χ, namely, $k_\chi = (1, 10)$; the best fit for the kinetic mixing parameter would then be $\epsilon_\phi \sim (10^{-8}, 10^{-9})$.

On the other hand, the significance of the DAMA region alone gets lower, due to the fact that for pure long range interaction ($q \gg m_\phi$) the $1/q^4$ drop-off of the unmodulated signal rapidly overshoots the measured total rate (see [41, Figure 1]), that of course we treat as an intrinsic constraint in our analysis. This can be appreciated in more details in Figure 4, where again the DAMA allowed regions are shown, but in the (m_χ, m_ϕ) plane. As one can see a 99% confidence level lower bound on the mass of the dark photon around 10 MeV is possible to be placed. This is due to the fact that the unmodulated signal, unlike the modulated one, is particularly sensitive to the energy drop-off of the cross section, which is typical for Rutherford-like scattering. The situation does not dramatically vary if we change the properties of the dark matter halo. Indeed, if we consider a more physical triaxial halo with the same velocity dispersion in the major axis (right plot of Figure 4), the allowed regions are only slightly enhanced.

Nevertheless, it is worth noticing that, in a dark world filled by more than one species in thermal equilibrium, the DM particles responsible for the annual modulation may possess smaller velocity dispersion. For instance, in the context of mirror DM, the dominant species can be the mirror hydrogen, like our world, while the mass of the DM particles favored by direct detection experiments is around 16 GeV (mirror oxigen). If they are in thermal equilibrium, the relation $v_0 = 1/\sqrt{2}\ (A_H/A_O)^{1/2} \cdot 220$ km/s $\lesssim$ 100 km/s then will hold [21]. In this case the constraints in Figure 4 are less important, because the raise of the total rate for low nuclear recoil energy is under threshold (see, e.g., [21, Figures 5(a) and 5(b)]).

Since, as already stated, the normalized total cross section and in turn the rate depend collectively on the kinetic mixing parameter ϵ_ϕ and on the DM-dark photon coupling k_χ; in the next section, a complementary class of constraints which are relevant for DM models featured by a long range interaction will be presented.

4.3. Complementary Constraints. A first class of complementary constraints that solely depends on the properties of the dark photon (kinetic mixing parameter ϵ_ϕ and its mass m_ϕ) is the one coming from beam dump neutrino experiments and supernovæ observations. In Figure 5 a compilation of the bounds in the (m_ϕ, ϵ_ϕ) plane is shown. Specifically,

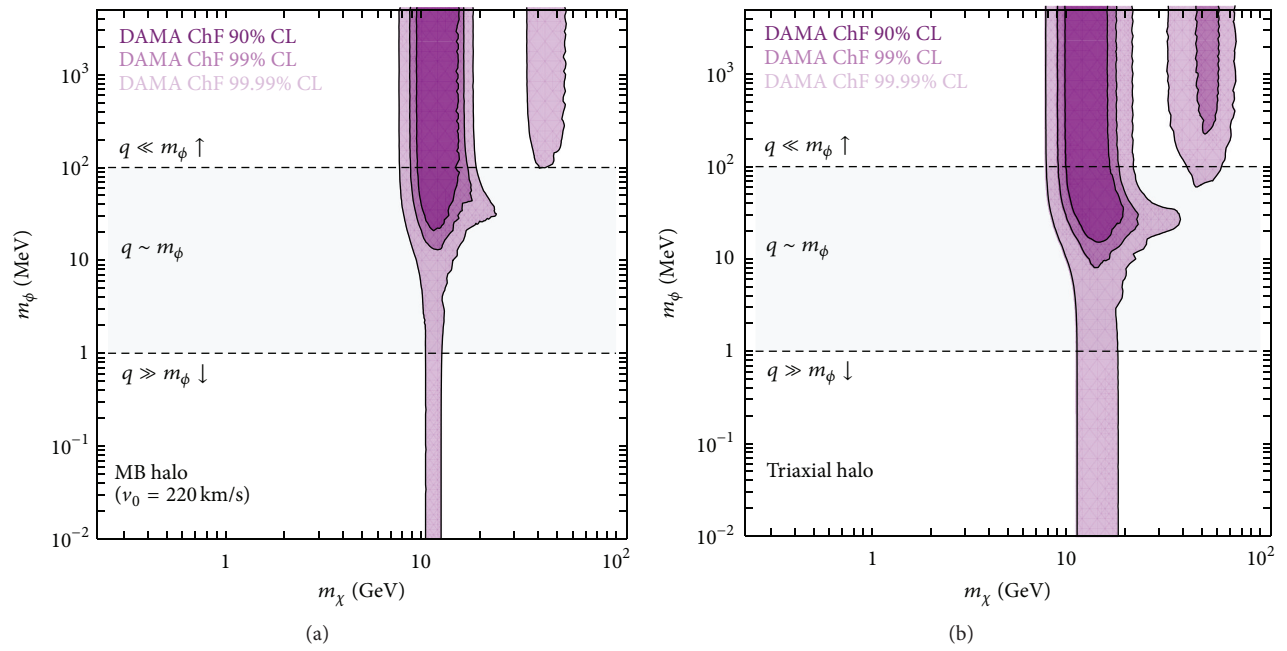

FIGURE 4: *The bounds on the mediator mass as a function of the DM one* obtained by comparing the DAMA modulated signal with the total rate. The allowed regions are reported for CLs of 90%, 99%, and 99.99% in shaded magenta. In (a) an isothermal sphere with velocity dispersion $v_0 = 220$ km/s and a local DM energy density $\rho_\odot = 0.3\,\text{GeV/cm}^3$ has been assumed. In (b) we instead show the allowed regions by considering a more physical triaxial halo with the same velocity dispersion in the major axis and with $\rho_\odot = 0.84\,\text{GeV/cm}^3$. These results have been presented in [24, 25].

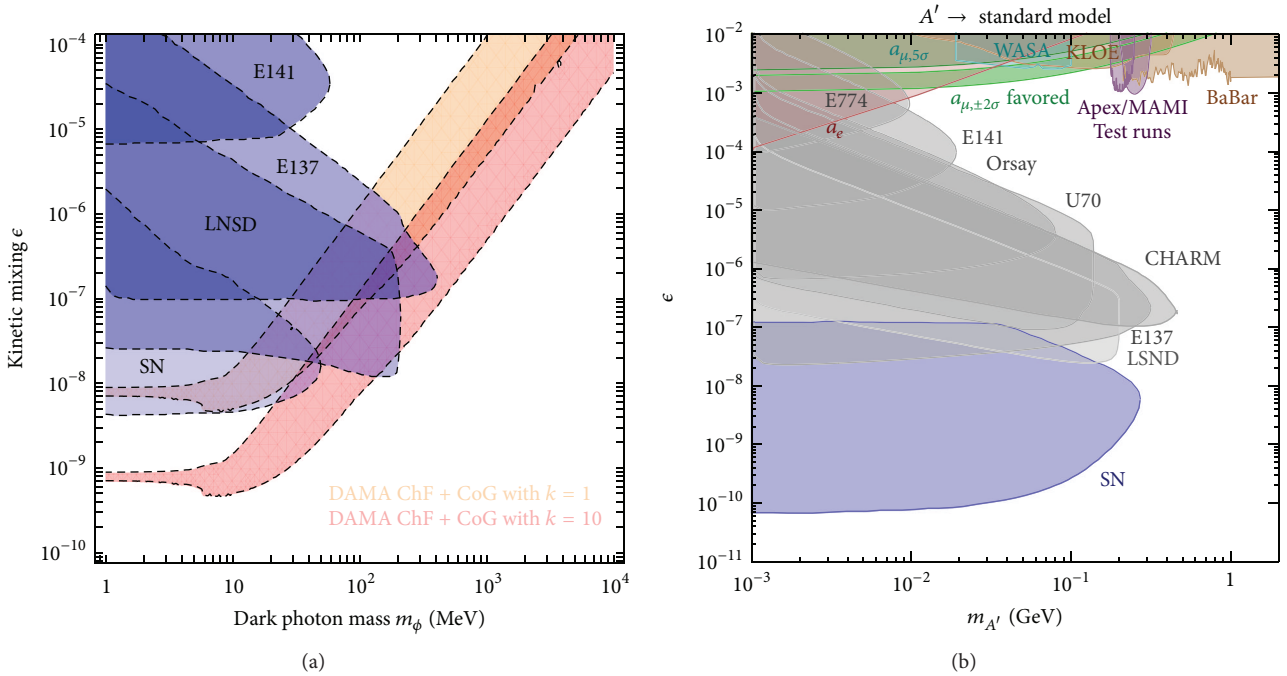

FIGURE 5: *Allowed regions and a compilation of constraints* in the (m_ϕ, ϵ_ϕ) plane. (a) The upper (orange) and the lower (red) allowed regions are derived by combining the DAMA and CoGeNT annual modulation dataset. Specifically, the absence of modulation is here rejected at 8σ CL. The two regions differ in the choice of parameter k_χ; namely $k_\chi = 1$ (upper) and $k_\chi = 10$ (lower). In blue are instead represented the constraints coming from beam dumped neutrino experiments and supernovæ observations taken from [95, 96]. (b) A compilation of the latest constraints in the (m_ϕ, ϵ_ϕ) plane. This plot has been taken from the following review [97]. It is worth pointing out that for $m_\phi \lesssim 10^{-6}$ eV the parameter space of the positive results experiments in direct DM searches is basically unbounded (see, e.g., [97, Figure 7]).

on the left panel the shaded blue regions are taken from [95, 96], while those in the right one represent the latest constraints on the dark photon properties presented in [97] (notice that the labels ϵ and $m_{A'}$ in the plots of Figure 5 stand for the kinetic mixing parameter ϵ_ϕ and the dark photon mass m_ϕ, resp.). As is apparent, the bounds coming from supernovæ observations (namely, the energy loss observed from SN1987a) are the most stringent. They exclude small kinetic mixing parameter and light mass for the dark photon. Indeed, in this case, if dark photons were produced in relevant amount in the centre of a supernova via mixing with the ordinary photon, the subsequent emission of them would shorten so that the predicted neutrinos boost that it would become inconsistent with the measurements made by KamiokaNDE (see, e.g., [95, 98, 99]).

The allowed regions of the DAMA and CoGeNT experiments projected in the (m_ϕ, ϵ_ϕ) plane are instead shown in the left plot of Figure 5. Since, as already stated, the normalization of the rate depends not only on the properties of the dark photon but also on its coupling with the DM particles, we present the results for two benchmark values of k_χ, for example, $k_\chi = 1$ (upper orange region) and $k_\chi = 10$ (lower orange region). We can see that, in the "symmetric" case $k_\chi = 1$, only the dark photons with $m_\phi \gtrsim 100\,\mathrm{MeV}$ can simultaneously satisfy the constraints and give a reasonable fit of the positive results of experiments. On the other hand, for $k_\chi \gtrsim 50$, the whole range is basically unbounded. It is worth stressing that such large values of k_χ can be easily obtained either in models of composite DM particles with large Z_χ (e.g., mirror models) or in those with a strongly coupled dark sector. Furthermore, it is also relevant to point out that, for pure long range interaction ($m_\phi = 0$), the majority of the bounds, and in particular those coming from supernovæ observations, do not apply, being the direct production of dark photon forbidden by kinematical reason (see, e.g., [97, Figure 7]).

A second class of constraints which instead solely depends on the properties on the dark sector itself is the one coming from the self-interactions. Indeed, since for this class of models the DM-DM scattering, given by

$$V(r) = \frac{\alpha k_\chi}{r} e^{-m_\phi r}, \tag{32}$$

is not suppressed by ϵ_ϕ, the self-interactions can easily reach high values, making the dynamics of virialized astrophysical objects affected. This is particularly relevant in the limit $m_\phi \to 0$; indeed, in this case the self-interaction (32) could be of the same order of the electromagnetic scattering.

A first example of such bounds comes from the observations of colliding galaxy clusters, like the bullet cluster [100], which points towards collision-less DM. In particular a quite robust bound $\langle \sigma_T \rangle / m_\chi \lesssim 1.25\,\mathrm{cm}^2/\mathrm{g}$ on the size of the self-interaction has been placed by [101]. In order to translate such bound in a constraint on the dark photon mass, one has to compute the weighted energy transfer cross section, which measures the rate at which energy is transferred in the system. It reads

$$\langle \sigma_T \rangle = \iint \mathrm{d}^3 v_1 \mathrm{d}^3 v_2 f(v_1) f(v_2) \sigma_T(v_{\mathrm{rel}}), \tag{33}$$

where $\sigma_T(v_{\mathrm{rel}}) = \int \mathrm{d}\Omega \mathrm{d}\sigma/\mathrm{d}\Omega (1 - \cos\theta)$ is the two-body energy transfer cross section. Here $f(v)$ is the DM velocity distribution, assumed to be Maxwellian, and $v_{\mathrm{rel}} = |\vec{v}_1 - \vec{v}_2|$ is the relative velocity of the DM particles involved in the scattering. Considering now the typical velocity of collision in the bullet cluster of 4700 km/s, a DM mass of 10 GeV, and two values of $k_\chi = (1, 10)$, the bound of $1.25\,\mathrm{cm}^2/\mathrm{g}$ is exceeded if the mass of the dark photon is smaller than (1, 20) MeV.

A second example of bounds, which is in principle relevant for this kind of models, comes from the fact that quite large self-interaction rapidly drives the DM halo into a spherical configuration, due to the prompt equipartition of the energy in the system. In particular, the efficiency of such process can be roughly estimated by

$$\tau_{\mathrm{rel}} = \frac{1}{\langle \Gamma_T \rangle}, \tag{34}$$

where

$$\langle \Gamma_T \rangle = \iint \mathrm{d}^3 v_1 \mathrm{d}^3 v_2 f(v_1) f(v_2) n_\chi v_{\mathrm{rel}} \sigma_T(v_{\mathrm{rel}}) \frac{v_{\mathrm{rel}}^2}{v_0^2}, \tag{35}$$

which is telling us the typical time at which the self-interactions affect the dynamics of a virialized astrophysical object with number density n_χ and dispersion velocity v_0. Indeed, if it is smaller than the age of the object, a spherical configuration will tend to form, making such scenario excluded by few elliptical DM halos observations [102–106]. In particular, in the case of galaxy clusters we get that the relaxation time is always bigger than the age of the object ($\tau_{\mathrm{ob}} \sim 10^{10}$ years), making therefore the mass of the dark photon basically unbounded. On the other hand, if we consider a smaller halo, like the one of dwarf galaxies, which are characterized by larger number density and smaller velocity dispersion, one can in principle put a very stringent lower bound on the mass of the dark photon of the order of 100 MeV (see also [107, 108]).

Nevertheless, it is worth stressing that the derivations of the constraints coming from self-interaction are affected by several uncertainties both from the theoretical and experimental side. Indeed, since the phenomenology of this class of models is completely different compared to the standard one, an N-body/hydrodynamical simulation is needed. This is especially true in the case of multicomponent dark sector, in which the different equipartitions of the energy among the DM particles can generate a sort of dark electric and magnetic fields in the long range regime. Furthermore, since the self-interaction needed to change their dynamics is in general of the order of the Thomson scattering ($\sigma_{\mathrm{em}} \sim 10^{-24}\,\mathrm{cm}^2$), from trivial analysis dimension of such large cross section, the following rough estimation yields: the self-interaction is of a long range type in most of the virialized astrophysical objects under the assumption that the DM-dark photon coupling is

of the order of α. In this case, the probability to radiate a dark photon in the scattering process is then different from zero and therefore it might well be possible that the DM sector is dissipative like ours. The time at which energy is transferred in the system ($\tau_{\rm rel}$) is no longer a good indicator, since the relevant quantity that describes the dynamical evolution of the system is now the cooling time: in particular, for a DM sector composed by heavy and light species, the dissipation time due to the soft emission of the dark photon (dark bremsstrahlung) can be smaller than the age of the virialized astrophysical objects (see, e.g., [109–111]). In this scenario the system is no longer stable, and in general it starts to collapse. By virtue of this fact, we do not consider this last class of constraints, since dedicated and careful analysis involving also numerical simulations is needed.

5. Conclusion

Direct DM searches are now characterized by tantalizing results and hints that make this field very active both from the theoretical and experimental side. In particular, in addition to the long standing DAMA results, nowadays there are other experiments, like CoGeNT, CRESST-II and CDMS-Si that are starting to observe anomalies in their counting rates. On the other hand, the increasingly stringent constraints coming from null result experiments put in serious trouble the theoretical interpretation of the data, at least in terms of the simple-minded SI contact interaction. In this work I discussed the *status* of direct DM detection with specific attention to the experimental results and their phenomenological interpretation in terms of DM interaction. In particular, in the first part I presented a new and more general approach to study signals in this field based on nonrelativistic operators. Then I reviewed the experimental results and their interpretation in terms of the "standard" SI interaction pointing out all the uncertainties which enter in this field. In the last part of this work, I investigated a fermionic dark matter particle carrying a small millicharged and analyzed its impact on direct detection experiments. I showed that this kind of long range interaction can accommodate the positive experimental results. By assuming a conservative choice for the lower threshold of the XENON100 and LUX experiments I have demonstrated that this candidate is not ruled out. I also determined the complementary class of constraints which are relevant for millicharged DM particles with long range forces.

Finally, I would like to propose a possible direction to pursue in order to make sense of the current exciting experimental panorama based on the formalism of nonrelativistic operators. Indeed, as we have seen in the first part of this work, it allows us to describe the DM-nucleus interactions in terms of a very limited number of relevant degrees of freedom. In this way, it is possible to parametrize the model-dependent part of the rate from the model-independent one encapsulated in a sort of *integrated form factors* that encode all the dependences on the astrophysics, nuclear physics, and experimental details. Therefore, since one is ignorant or agnostic about the underlying theory, I would like to encourage a synergy between nuclear physicists and experimentalists in order to provide a complete set of *integrated form factors* defined in (23). It would be extremely useful for the community, because, in this way, one can compute the expected number of events for any kind of interaction (e.g., including isospin-violating interactions, momentum-dependent form factors, and velocity-dependent form factors) and compare it directly with the experimental results. Providing the *integrated form factors* will thus be the first step towards a model-independent analysis in direct DM searches.

Conflict of Interests

The author declares that there is no conflict of interests regarding the publication of this paper.

Acknowledgments

The author thanks Marco Cirelli, Eugenio Del Nobile, and Joe Silk for useful discussions.

References

[1] P. A. R. Ade, N. Aghanim, C. Armitage-Caplan et al., "Planck 2013 results. XVI: cosmologicalparameters," http://arxiv.org/abs/1303.5076.

[2] G. Bertone, D. Hooper, and J. Silk, "Particle dark matter: evidence, candidates and constraints," *Physics Reports*, vol. 405, no. 5-6, pp. 279–390, 2 5.

[3] G. Jungman, M. Kamionkowski, and K. Griest, "Supersymmetric dark matter," *Physics Report*, vol. 267, no. 5-6, pp. 195–373, 1996.

[4] J. Beringer, J. F. Arguin, R. M. Barnett et al., "Review of particle physics," *Physical Review D*, vol. 86, no. 1, Article ID 01 01, 2012.

[5] R. Catena and P. Ullio, "A novel determination of the local dark matter density," *Journal of Cosmology and Astroparticle Physics*, vol. 2010, no. 8, article 4, 2010.

[6] M. Weber and W. De Boer, "Determination of the local dark matter density in our galaxy," *Astronomy and Astrophysics*, vol. 509, no. 1, A25, 2010.

[7] P. Salucci, F. Nesti, G. Gentile, and C. F. Martins, "The dark matter density at the Sun's location," *Astronomy and Astrophysics*, vol. 523, no. 5, article A83, 2010.

[8] D. Lynden-Bell and S. Jin, "Statistical mechanics of violent relaxation in stellar systems," *Monthly Notices of the Royal Astronomical Society*, vol. 136, no. 1, p. 101, 1967.

[9] M. Vogelsberger, A. Helmi, V. Springel et al., "Phase-space structure in the local dark matter distribution and its signature in direct detection experiments," *Monthly Notices of the Royal Astronomical Society*, vol. 395, no. 2, pp. 797–811, 2009.

[10] Y. P. Jing and Y. Suto, "Triaxial modeling of halo density profiles with high-resolution N-body simulations," *Astrophysical Journal Letters*, vol. 574, no. 2, pp. 538–553, 2 2.

[11] C. Savage, G. Gelmini, P. Gondolo, and K. Freese, "Compatibility of DAMA/LIBRA dark matter detection with other searches," *Journal of Cosmology and Astroparticle Physics*, vol. 2 9, no. 4, article 010, 2 9.

[12] P. Belli, R. Cerulli, N. Fornengo, and S. Scopel, "Effect of the galactic halo modeling on the DAMA-NaI annual modulation

result: an extended analysis of the data for weakly interacting massive particles with a purely spin-independent coupling," *Physical Review D*, vol. 66, no. 4, Article ID 043503, 2002.

[13] N. Fornengo and S. Scopel, "Temporal distortion of the annual modulation signal of weakly interacting massive particles at low recoil energies," *Physics Letters B*, vol. 576, no. 1-2, pp. 189–194, 2003.

[14] A. K. Drukier, K. Freese, and D. N. Spergel, "Detecting cold dark-matter candidates," *Physical Review D*, vol. 33, no. 12, pp. 3495–3508, 1986.

[15] K. Freese, J. Frieman, and A. Gould, "Signal modulation in cold-dark-matter detection," *Physical Review D*, vol. 37, no. 12, pp. 3388–3405, 1988.

[16] B. A. Dobrescu and I. Mocioiu, "Spin-dependent macroscopic forces from new particle exchange," *Journal of High Energy Physics*, vol. 2006, no. 11, article 005, 2006.

[17] A. L. Fitzpatrick, W. Haxton, E. Katz, N. Lubbers, and Y. Xu, "The effective field theory of dark matter direct detection," *Journal of Cosmology and Astroparticle Physics*, vol. 2013, no. 2, article 004, 2013.

[18] A. L. Fitzpatrick, W. Haxton, E. Katz, N. Lubbers, and Y. Xu, "Model independent direct detection analyses," http://arxiv.org/abs/1211.2818.

[19] N. Anand, A. L. Fitzpatrick, and W. C. Haxton, "Model-independent WIMP scattering responses and event rates: a mathematica package for experimental analysis," http://arxiv.org/abs/1308.6288.

[20] M. Pospelov and T. Ter Veldhuis, "Direct and indirect limits on the electro-magnetic form factors of WIMPs," *Physics Letters B*, vol. 480, no. 1-2, pp. 181–186, 2000.

[21] R. Foot, "Mirror dark matter and the new DAMA/LIBRA results: a simple explanation for a beautiful experiment," *Physical Review D*, vol. 78, no. 4, Article ID 043529, 10 pages, 2008.

[22] R. Foot, "A CoGeNT confirmation of the DAMA signal," *Physics Letters B*, vol. 692, no. 2, pp. 65–69, 2010.

[23] R. Foot, "Mirror & hidden sector dark matter in the light of new CoGeNT data," *Physics Letters B*, vol. 703, no. 1, pp. 7–13, 2011.

[24] N. Fornengo, P. Panci, and M. Regis, "Long-range forces in direct dark matter searches," *Physical Review D*, vol. 84, no. 11, Article ID 115002, 2011.

[25] P. Panci, http://arxiv.org/abs/1206.2240.

[26] D. E. Kaplan, G. Z. Krnjaic, K. R. Rehermann, and C. M. Wells, "Atomic dark matter," *Journal of Cosmology and Astroparticle Physics*, vol. 2010, no. 5, article 021, 2010.

[27] K. Sigurdson, M. Doran, A. Kurylov, R. R. Caldwell, and M. Kamionkowski, "Dark-matter electric and magnetic dipole moments," *Physical Review D*, vol. 70, no. 8, Article ID 083501, 15 pages, 2004, Erratum in *Physical Review D*, vol. 73, no. 8, Article ID 089903, 2006.

[28] S. Chang, N. Weiner, and I. Yavin, "Magnetic inelastic dark matter," *Physical Review D*, vol. 82, no. 12, Article ID 125011, 2010.

[29] V. Barger, W. Y. Keung, and D. Marfatia, "Electromagnetic properties of dark matter: dipole moments and charge form factor," *Physics Letters B*, vol. 696, no. 1-2, pp. 74–78, 2011.

[30] E. Del Nobile, C. Kouvaris, P. Panci, F. San- nino, and J. Virkajarvi, "Light magnetic dark matter in direct detection searches," *Journal of Cosmology and Astroparticle Physics*, vol. 2012, no. 8, article 10, 2012.

[31] C. M. Ho and R. J. Scherrer, "Anapole dark matter," *Physics Letters B*, vol. 722, no. 4-5, pp. 341–346, 2013.

[32] M. Cirelli, E. Del Nobile, and P. Panci, "Tools for model-independent bounds in direct dark matter searches," *Journal of Cosmology and Astroparticle Physics*, vol. 2013, no. 10, article 019, 2013.

[33] R. H. Helm, "Inelastic and elastic scattering of 187-Mev electrons from selected even-even nuclei," *Physical Review*, vol. 104, no. 5, pp. 1466–1475, 1956.

[34] R. Bernabei, P. Belli, V. Landoni et al., "New limits on WIMP search with large-mass low-radioactivity NaI(T1) set-up at Gran Sasso," *Physics Letters B*, vol. 389, no. 4, pp. 757–766, 1996.

[35] R. Bernabei, P. Belli, F. Montecchia et al., "Possible implications of the channeling effect in NaI(Tl) crystals," *European Physical Journal C*, vol. 53, no. 2, pp. 205–213, 2008.

[36] E. M. Drobyshevski, "Channeling effect and improvement of the efficiency of charged particle registration with crystal scintillators," *Modern Physics Letters A*, vol. 23, no. 36, pp. 3077–3085, 2008.

[37] J. Graichen, K. Maier, J. Schüth, A. Siepe, and W. Von Witsch, "Efficiency and directional effects in the detection of low-energy recoil nuclei in a NaI(Tl) single crystal," *Nuclear Instruments and Methods in Physics Research A*, vol. 485, no. 3, pp. 774–779, 2002, Erratum in *Nuclear Instruments and Methods in Physics Research A*, vol. 501, no. 2-3, p. 630, 2003.

[38] B. Feldstein, A. L. Fitzpatrick, E. Katz, and B. Tweedie, "A simple explanation for DAMA with moderate channeling," *Journal of Cosmology and Astroparticle Physics*, vol. 2010, no. 3, article 029, 2010.

[39] N. Bozorgnia, G. B. Gelmini, and P. Gondolo, "Channeling in direct dark matter detection I: channeling fraction in NaI (Tl) crystals," *Journal of Cosmology and Astroparticle Physics*, vol. 2010, no. 11, article 019, 2010.

[40] J. I. Collar, "Quenching and channeling of nuclear recoils in NaI(Tl): implications for dark-matter searches," *Physical Review C*, vol. 88, no. 3, Article ID 035806, 9 pages, 2013.

[41] R. Bernabei, P. Belli, F. Cappella et al., "First results from DAMA/LIBRA and the combined results with DAMA/NaI," *European Physical Journal C*, vol. 56, no. 3, pp. 333–355, 2008.

[42] R. Bernabei, P. Belli, F. Cappella et al., "New results from DAMA/LIBRA," *European Physical Journal C*, vol. 67, no. 1, pp. 39–49, 2010.

[43] P. S. Barbeau, J. I. Collar, and O. Tench, "Large-mass ultralow noise germanium detectors: performance and applications in neutrino and astroparticle physics," *Journal of Cosmology and Astroparticle Physics*, vol. 2007, no. 9, article 009, 2007.

[44] C. E. Aalseth, P. S. Barbeau, N. S. Bowden et al., "Results from a search for light-mass dark matter with a p-type point contact germanium detector," *Physical Review Letter*, vol. 106, no. 13, Article ID 131301, 4 pages, 2011.

[45] C. E. Aalseth, P. S. Barbeau, J. Colaresi et al., "Search for an annual modulation in a p-type point contact Germanium dark matter detector," *Physical Review Letters*, vol. 107, no. 14, Article ID 141301, 2011.

[46] C. E. Aalseth, P. S. Barbeau, J. Colaresi et al., "Search for an annual modulation in three years of CoGeNT dark matter detector data," http://arxiv.org/abs/1401.3295.

[47] C. E. Aalseth, P. S. Barbeau, J. Colaresi et al., "Search for an annual modulation in a p-type point contact Germanium dark matter detector," *Physical Review Letters*, vol. 107, no. 14, Article ID 141301, 2011.

[48] G. Angloher, M. Bauer, I. Bavykina et al., "Results from 730 kg days of the CRESST-II Dark Matter Search," *The European Physical Journal C*, vol. 2012, article 1971, 2012.

[49] Z. Ahmed, D. S. Akerib, S. Arrenberg et al., "Dark matter search results from the CDMS II experiment," *Science*, vol. 327, pp. 1619–1621, 2010.

[50] R. Agnese, Z. Ahmed, A. J. Anderson et al., "Silicon detector results from the first five-tower run of CDMS II," *Physical Review D*, vol. 88, no. 3, Article ID 031104, 5 pages, 2013.

[51] R. Agnese, Z. Ahmed, A. J. Anderson et al., "Silicon detector dark matter results from the final exposure of CDMS II," *Physical Review Letters*, vol. 111, no. 25, Article ID 251301, 6 pages, 2013.

[52] J. Angle, E. Aprile, F. Arneodo et al., "First results from the XENON10 dark matter experiment at the Gran Sasso National Laboratory," *Physical Review Letter*, vol. 100, no. 2, Article ID 021303, 5 pages, 2008.

[53] E. Aprile, M. Alfonsi, K. Arisaka et al., "Dark matter results from 225 live days of XENON100 data," *Physical Review Letter*, vol. 109, no. 18, Article ID 181301, 6 pages, 2012.

[54] D. S. Akerib, H. M. Araujo, X. Bai et al., "First results from the LUX dark matter experiment at the sanford underground research facility," http://arxiv.org/abs/1310.8214.

[55] E. Behnke, J. Behnke, S. J. Brice et al., "First dark matter search results from a 4-kg CF3I bubble chamber operated in a deep underground site," *Physical Review D*, vol. 86, no. 5, Article ID 052001, 9 pages, 2012.

[56] T. Schwetz and J. Zupan, "Dark matter attempts for CoGeNT and DAMA," *Journal of Cosmology and Astroparticle Physics*, vol. 2011, no. 8, article 008, 2011.

[57] M. Farina, D. Pappadopulo, A. Strumia, and T. Volansky, "Can CoGeNT and DAMA modulations be due to Dark Matter?" *Journal of Cosmology and Astroparticle Physics*, vol. 2011, no. 11, article 010, 2011.

[58] P. J. Fox, J. Kopp, M. Lisanti, and N. Weiner, "A CoGeNT modulation analysis," *Physical Review D*, vol. 85, no. 3, Article ID 036008, 2012.

[59] D. Hooper and C. Kelso, "Implications of CoGeNT's new results for dark matter," *Physical Review D*, vol. 84, no. 8, Article ID 083001, 10 pages, 2011.

[60] P. Gondolo, P. Ko, and Y. Omura, "Light dark matter in leptophobic $Z\prime$ models," *Physical Review D*, vol. 85, no. 3, Article ID 035022, 2012.

[61] E. Del Nobile, C. Kouvaris, and F. Sannino, "Interfering composite asymmetric dark matter as explanation for DAMA and CoGeNT results," *Physical Review D*, vol. 84, no. 2, Article ID 027301, 4 pages, 2011.

[62] C. Arina, J. Hamann, and Y. Y. Y. Wong, "A Bayesian view of the current status of dark matter direct searches," *Journal of Cosmology and Astroparticle Physics*, vol. 2011, no. 9, article 022, 2011.

[63] M. T. Frandsen, F. Kahlhoefer, J. March-Russell, C. McCabe, M. McCullough, and K. Schmidt-Hoberg, "On the DAMA and CoGeNT modulations," *Physical Review D*, vol. 84, no. 4, Article ID 041301, 2011.

[64] J. L. Feng, J. Kumar, D. Marfatia, and D. Sanford, "Isospin-violating dark matter," *Physics Letters B*, vol. 703, no. 2, pp. 124–127, 2011.

[65] D. Hooper, J. I. Collar, J. Hall, D. McKinsey, and C. M. Kelso, "Consistent dark matter interpretation for CoGeNT and DAMA/LIBRA," *Physical Review D*, vol. 82, no. 12, Article ID 123509, 2010.

[66] S. Chang, J. Liu, A. Pierce, N. Weiner, and I. Yavin, "CoGeNT interpretations," *Journal of Cosmology and Astroparticle Physics*, vol. 2010, no. 8, article 018, 2010.

[67] A. L. Fitzpatrick, D. Hooper, and K. M. Zurek, "Implications of CoGeNT and DAMA for light WIMP dark matter," *Physical Review D*, vol. 81, no. 11, Article ID 115005, 2010.

[68] J. Kopp, T. Schwetz, and J. Zupan, "Global interpretation of direct Dark Matter searches after CDMS-II results," *Journal of Cosmology and Astroparticle Physics*, vol. 2010, no. 2, article 014, 2010.

[69] P. J. Fox, J. Liu, and N. Weiner, "Integrating out astrophysical uncertainties," *Physical Review D*, vol. 83, no. 10, Article ID 103514, 12 pages, 2011.

[70] P. J. Fox, G. D. Kribs, and T. M. P. Tait, "Interpreting dark matter direct detection independently of the local velocity and density distribution," *Physical Review*, vol. 83, no. 3, Article ID 034007, 12 pages, 2011.

[71] C. McCabe, "DAMA and CoGeNT without astrophysical uncertainties," *Physical Review D*, vol. 84, no. 4, Article ID 043525, 6 pages, 2011.

[72] J. Herrero-Garcia, T. Schwetz, and J. Zupan, "On the annual modulation signal in dark matter direct detection," *Journal of Cosmology and Astroparticle Physics*, vol. 2012, no. 3, article 005, 2012.

[73] J. Herrero-Garcia, T. Schwetz, and J. Zupan, "Astrophysics-independent bounds on the annual modulation of dark matter signals," *Physical Review Letter*, vol. 109, no. 14, Article ID 141301, 5 pages, 2012.

[74] M. T. Frandsen, F. Kahlhoefer, C. McCabe, S. Sarkar, and K. Schmidt-Hoberg, "Resolving astrophysical uncertainties in dark matter direct detection," *Journal of Cosmology and Astroparticle Physics*, vol. 2012, no. 1, article 024, 2012.

[75] P. Gondolo and G. B. Gelmini, "Halo independent comparison of direct dark matter detection data," *Journal of Cosmology and Astroparticle Physics*, vol. 2012, no. 12, article 015, 2012.

[76] M. T. Frandsen, F. Kahlhoefer, C. McCabe, S. Sarkar, and K. Schmidt-Hoberg, "The unbearable lightness of being: CDMS versus XENON," *Journal of Cosmology and Astroparticle Physics*, vol. 2013, no. 7, article 023, 2013.

[77] E. Del Nobile, G. B. Gelmini, P. Gondolo, and J. H. Huh, "Halo-independent analysis of direct detection data for light WIMPs," *Journal of Cosmology and Astroparticle Physics*, vol. 2013, no. 10, article 026, 2013.

[78] N. Bozorgnia, J. Herrero-Garcia, T. Schwetz, and J. Zupan, "Halo-independent methods for inelastic dark matter scattering," *Journal of Cosmology and Astroparticle Physics*, vol. 2013, no. 7, article 049, 2013.

[79] E. Del Nobile, G. Gelmini, P. Gondolo, and J. H. Huh, "Generalized halo independent comparison of direct dark matter detection data," *Journal of Cosmology and Astroparticle Physics*, vol. 2013, no. 10, article 048, 2013.

[80] E. Del Nobile, G. B. Gelmini, P. Gondolo, and J. H. Huh, "Update on light WIMP limits: LUX, lite and light," http://arxiv.org/abs/1311.4247.

[81] T. D. Lee and C. N. Yang, "Question of parity conservation in weak interactions," *Physical Review*, vol. 104, no. 1, pp. 254–258, 1956.

[82] I. Kobzarev, L. Okun, and I. Pomeranchuk, "On the possibility of observing mirror particle," *Soviet Journal of Nuclear Physics*, vol. 3, p. 837, 1966.

[83] S. I. Blinnikov and M. Y. Khlopov, "Possible signatures of mirror particles," *Soviet Journal of Nuclear Physics*, vol. 36, pp. 472–474, 1982.

[84] S. I. Blinnikov and M. Khlopov, "Possible astronomical effects of mirror particles," *Astronomicheskii Zhurnal*, vol. 60, pp. 632–639, 1983.

[85] Z. Berezhiani, "Marriage between the baryonic and dark matters," *AIP Conference Proceedings*, vol. 878, pp. 195–202, 2006.

[86] R. Foot, "Mirror matter-type dark matter," *International Journal of Modern Physics D*, vol. 13, no. 10, pp. 2161–2192, 2004.

[87] Z. Berezhiani, "Through the looking-glass: Alice's adventures in mirror world," in *From Fields to Strings: Circumnavigating Theoretical Physics*, M. Shifman, A. Vainshtein, and J. Wheater, Eds., vol. 3, pp. 2147–2195, World Scientific.

[88] B. Holdom, "Two U(1)'s and ϵ charge shifts," *Physics Letters B*, vol. 166, no. 2, pp. 196–198, 1986.

[89] R. Foot, H. Lew, and R. R. Volkas, "A model with fundamental improper spacetime symmetries," *Physics Letters B*, vol. 272, no. 1-2, pp. 67–70, 1991.

[90] R. Foot, A. Y. Ignatiev, and R. R. Volkas, "Physics of mirror photons," *Physics Letters B*, vol. 503, no. 3-4, pp. 355–361, 2001.

[91] P. Belli, R. Bernabei, A. Bottino et al., "Observations of annual modulation in direct detection of relic particles and light neutralinos," *Physical Review D*, vol. 84, no. 5, Article ID 055014, 2011.

[92] E. Aprile, F. Arneodo, A. Askin et al., "Dark matter results from 100 live days of XENON100 data," *Physical Review Letter*, vol. 107, no. 13, Article ID 131302, 6 pages, 2011.

[93] R. Bernabei, P. Belli, A. Incicchitti, and D. Prosperi, "Liquid noble gases for dark matter searches: a synoptic survey," http://arxiv.org/abs/0806.0011.

[94] J. I. Collar, "A realistic assessment of the sensitivity of XENON10 and XENON100 to light-mass WIMPs," http://arxiv.org/abs/1106.0653.

[95] J. D. Bjorken, R. Essig, P. Schuster, and N. Toro, "New fixed-target experiments to search for dark gauge forces," *Physical Review D*, vol. 80, no. 7, Article ID 075018, 2009.

[96] R. Essig, R. Harnik, J. Kaplan, and N. Toro, "Discovering new light states at neutrino experiments," *Physical Review D*, vol. 82, no. 11, Article ID 113008, 2010.

[97] R. Essig, J. A. Jaros, W. Wester et al., "Dark sectors and new, light, weakly-coupled particles," http://arxiv.org/abs/1311.0029.

[98] J. B. Dent, F. Ferrer, and L. M. Krauss, "Constraints on light hidden sector gauge bosons from supernova cooling," http://arxiv.org/abs/1201.2683.

[99] H. K. Dreiner, J. F. o. Fortin, C. Hanhart, and L. Ubaldi, "Supernova constraints on MeV dark sectors from e+ e- annihilations," http://arxiv.org/abs/1310.3826.

[100] D. Clowe, M. Bradac, A. H. Gonzalez et al., "A direct empirical proof of the existence of dark matter," *The Astrophysical Journal Letters*, vol. 648, no. 2, pp. L109–L113, 2006.

[101] S. W. Randall, M. Markevitch, D. Clowe, A. H. Gonzalez, and M. Bradač, "Constraints on the self-interaction cross section of dark matter from numerical simulations of the merging galaxy cluster 1E 0657-56," *Astrophysical Journal Letters*, vol. 679, no. 2, pp. 1173–1180, 2008.

[102] J. L. Feng, M. Kaplinghat, H. Tu, and H. B. Yu, "Hidden charged dark matter," *Journal of Cosmology and Astroparticle Physics*, vol. 2009, no. 7, article 004, 2009.

[103] J. L. Feng, M. Kaplinghat, and H. B. Yu, "Halo-shape and relic-density exclusions of sommerfeld-enhanced dark matter explanations of cosmic ray excesses," *Physical Review Letters*, vol. 104, no. 15, Article ID 151301, 2010.

[104] M. R. Buckley and P. J. Fox, "Dark matter self-interactions and light force carriers," *Physical Review D*, vol. 81, no. 8, Article ID 083522, 9 pages, 2010.

[105] M. Ibe and H. B. Yu, "Distinguishing dark matter annihilation enhancement scenarios via halo shapes," *Physics Letters B*, vol. 692, no. 2, pp. 70–73, 2010.

[106] A. Loeb and N. Weiner, "Cores in dwarf galaxies from dark matter with a Yukawa potential," *Physical Review Letters*, vol. 106, no. 17, Article ID 171302, 2011.

[107] M. Kaplinghat, S. Tulin, and H. B. Yu, "Direct detection portals for self-interacting dark matter," http://arxiv.org/abs/1310.7945.

[108] S. Tulin, H. B. Yu, and K. M. Zurek, "Beyond collisionless dark matter: particle physics dynamics for dark matter halo structure," *Physical Review D*, vol. 87, no. 11, Article ID 115007, 20 pages, 2013.

[109] J. Fan, A. Katz, L. Randall, and M. Reece, "Double-disk dark matter," *Physics of the Dark Universe*, vol. 2, no. 3, pp. 139–156, 2013.

[110] J. Fan, A. Katz, L. Randall, and M. Reece, "Dark-disk universe," *Physical Review Letter*, vol. 110, no. 21, Article ID 211302, 5 pages, 2013.

[111] M. McCullough and L. Randall, "Exothermic double-disk dark matter," *Journal of Cosmology and Astroparticle Physics*, vol. 2013, no. 10, article 058, 2013.